Supporting Information

Rational Design of Iridium–Porphyrin Conjugates for Novel Synergistic Photodynamic and Photothermal Therapy Anticancer Agents

Liping Zhang,[†a] Yun Geng,[†a] Lijuan Li,[a] Xiaofan Tong,[a] Shi Liu,[a] Xingman Liu,[b] Zhongmin Su,[a] Zhigang Xie,*[b] Dongxia Zhu*[a] and Martin R. Bryce*[c]

[a] Key Laboratory of Nanobiosensing and Nanobioanalysis at Universities of Jilin Province, Department of Chemistry, Northeast Normal University, 5268 Renmin Street, Changchun, Jilin Province 130024, P. R. China. E-mail: zhudx047@nenu.edu.cn

[b] State key laboratory of Polymer Physics and Chemistry. Changchun Institute of Applied Chemistry Chinese Academy of Sciences. Changchun, 130022, P. R. China. E-mail: xiez@ciac.ac.cn

[c] Department of Chemistry, Durham University, Durham, DH1 3LE, UK.

E-mail: m.r.bryce@durham.ac.uk

Experimental Procedures

1. General information and methods

Materials

Materials obtained from commercial suppliers were used without further purification unless otherwise stated. All glassware, syringes, magnetic stirring bars and needles were thoroughly dried in a convection oven. All other materials for organic synthesis were purchased from Energy Chemical Company. 1,2-Distearoyl-*sn*-glycero-3-phosphoethanolamine-*N*-[maleimide(polyethylene glycol)-2000](DSPE-PEG-Mal) was provided by Shanghai Ponsure Biotech, Inc. HIV-1 transactivator of transcription (Tat) protein-derived cell penetrating peptide (C-terminus with cysteine) was purchased from GL Biochem Co., Ltd. (Shanghai, China). Dulbecco's Modified Eagle Medium (DMEM), RPMI-1640 Medium, and fetal bovine serum (FBS) were purchased from Sigma-Aldrich. 2',7'-Dichlorofluorescin diacetate (DCFH-DA) were purchased from Shanghai Beyotime Biotechnology Co., Ltd. 3-(4,5-Dimethylthiazol-2-yl)-2,5-diphenyltetrazolium bromide (MTT) was obtained from Shanghai Beyotime Biotechnology Co., Ltd. (China). The cell viability (live dead cell staining) assay kit was purchased from Jiangsu KeyGEN Biotechnology Co., Ltd. (China). Milli-Q water was collected from a Milli-Q system (Millipore).

Measurements

Reactions were monitored using thin layer chromatography (TLC). ^{1}H and ^{13}C NMR spectra were recorded at 25 ^{o}C on a Varian 500 MHz spectrometer. The chemical shifts (δ) are given in parts per million relative to internal standard TMS. The ^{1}H NMR spectra were referenced internally to the residual proton resonance of $CHCl_3$ in $CDCl_3$ (δ 7.24 ppm). The mass spectra (MS) of the samples were obtained on a Bruker autoflex III smart beam mass spectrometer (MALDI-TOF/TOF) with a smart beam laser at 355 nm wavelength. Elemental analysis was performed on a FlashEA1112 analyzer. UV–vis absorption spectra were monitored with a Shimadzu UV-2450 PC UV–vis spectrophotometer. Emission spectra were recorded on an Edinburgh FLS920 spectrofluorimeter under air at room temperature. Size and size

distribution (DLS) of the nanoparticles were characterized by a Malvern Zeta-sizer Nano instrument. Transmission electron microscopy (TEM) images were taken by a TECNAI F20 microscope. Confocal laser scanning microscopic (CLSM) images were obtained on a Zeiss Laser Scanning Confocal Microscope; LSM710. The mouse was imaged by using a Maestro *in vivo* optical imaging system (Cambridge Research & Instrumentation, Inc., Woburn, Massachusetts).

Density functional theory calculations

All the geometrical optimizations and TDDFT calculations for vertical excitation were performed using B3LYP functional and the 6-31G* basis set for H, C, N, O atoms, and the Hay-Wadt effective core potential (ECP) and a double-ξ basis set LANL2DZ for iridium atom. The molecular orbital information including energy levels and distribution was obtained at the same theoretical level. The above calculations were carried out in Gaussian 16 C01 program package.[1] The spin-orbital coupling (SOC) matrix elements for **TPP** and **1-Ir** were evaluated with zero-order regular approximation (ZORA) Hamiltonian in scalar approximation in the ADF code.[2] All-electron TZP basis sets were applied for the spin orbit coupling (SOC) calculation.

Preparation of nanoparticles

The **TPP** or **1-Ir** or **4-Ir** (1 mg) and 1,2-distearoyl-*sn*-glycero-3-phosphoethanolamine-*N*-[maleimide(polyethylene glycol)-2000](DSPE-PEG-Mal) (2 mg) were dissolved in THF (1 mL), and then poured into Milli-Q water (10 mL), followed by sonication for 2 min with a microtip probe sonicator (XL2000, Misonix Incorporated, NY). The residual THF solvent was evaporated by violent stirring of the suspension overnight. Subsequently, HIV-1 Tat (500 μg/mL, 150 μL) was added into the above solution and stirred at room temperature for 12 h. The excess HIV-1 Tat was removed by dialysis using a 10 000 molecular weight cutoff membrane. NPs were obtained by filtration through a 0.2 μm syringe-driven filter.

Singlet Oxygen Generation Measurements

To evaluate the $^1O_2$ generation ability of **TPP**/**1-Ir**/**4-Ir** NPs, a chemical method using DPBF as reactive oxygen species indicator was employed and monitored by UV–vis absorption spectroscopy. **TPP/1-Ir/4-Ir** NPs (1×10^{-6} M) were blended with a DPBF solution (1.5×10^{-5} M) and then irradiated with a 635 nm

laser at 0.4 W cm^{-2}. The absorption intensity of the DPBF at the maximum wavelength of 415 nm was detected every 10 s. The same experiments were done with free DPBF as a blank control.

Photothermal activity of PSs

The **TPP/1-Ir/4-Ir NPs** dispersions (6×10^{-5} M and 300 μL, respectively) were irradiated with a 635 nm laser at intensity of 0.8 W cm^{-2} for 300 s. Deionized water was measured as a control at the same conditions. Different concentrations and different laser intensity were used to verify the favorable photothermal activity of **4-Ir** NPs. The **4-Ir** NPs in solution with various concentrations (1×10^{-5} M, 2×10^{-5} M, 4×10^{-5} M, 6×10^{-5} M) were irradiated with 635 nm laser at a power density of 0.8 W cm^{-2} for 300 s and the **4-Ir** NPs dispersions (6×10^{-5} M, 300 μL) were also irradiated with 635 nm laser at different power densities (0.2, 0.4, 0.6, 0.8 W cm^{-2}) for 300 s. More precisely, the temperature changes of the solution were monitored by a thermocouple probe. The thermocouple probe and the laser path kept a parallel direction. A secure digital (SD) card was used to record the data every 10 s.

Photothermal conversion efficiency of PSs

The photothermal conversion efficiency of the NPs was calculated according to a reported method.[3] First, the **4-Ir** NPs (6×10^{-5} M) in solution were irradiated with 635 nm laser (0.8 W cm^{-2}) for 300 s and then the laser was turned off. After about 600 s, the solution was cooled to room temperature. The photothermal conversion efficiency (η) was calculated according to the following equation

$$\eta = \frac{hA(T_{Max}-T_{Min})-Q_{dis}}{1(1-10^{-A635})} \quad (1)$$

where h and A respectively represent the heat transfer coefficient and the surface area of the container, T_{Max} and T_{Min} represent the maximum temperature and the room temperature of the environment, Q_{dis} represents the heat dissipation of the solvent (water), I is the laser power employed (0.8 W cm^{-2}), and A_{635} is the absorbance of PS NPs at 635 nm. The value of hA is calculated from the following equation

$$\tau_S = \frac{m_D c_D}{hA} \quad (2)$$

where τ_s is the time constant for heat transfer of the system. mD and cD are the mass (300 μg) and heat capacity (4.2 J g^{-1}), respectively, of the deionized water used to disperse the NPs. Q_{dis} represents the heat

dissipation from the laser absorbed by the water, consequently *Q*dis was calculated according to the following equation

$$Q_{dis} = \frac{m_D c_D (T_{Max(water)} - T_{surr})}{\tau_{s(water)}} \quad (3)$$

Cell culture

HeLa cells (the human cervical cancer cell line) and U14 cells (the murine hepatic carcinoma cell line) were purchased from Jilin University and grown in Dulbecco's modified Eagle's medium (DMEM, GIBCO) supplemented with 10% heat-inactivated fetal bovine serum (FBS, GIBCO), 100 units/mL penicillin and 100 μg/mL streptomycin (Sigma). The cells were maintained in a humidified incubator at 37 °C with 5% CO_2.

Cytotoxicity assay

HeLa cells were harvested in a logarithmic growth phase and seeded in 96-well plates at a density of 10^4 cells per well for 24 h. Then different concentrations of **TPP/1-Ir/4-Ir** and **TPP/1-Ir/4-Ir** NPs of various concentrations (0-0.5 μM) were added into the cell culture medium separately. After incubating for 6 h, the light group was irradiated with a 635 nm laser (0.6 W cm^{-2}) for 5 min, then incubation was continued to 24 h. The dark control group received nothing and were incubated for the same time as the control group. Subsequently MTT (20 μL) was added to the medium for 4 h. The absorbance of MTT was measured by a Bio-Rad 680 microplate reader at 490 nm.

Intracellular ROS assays

HeLa cells were seeded in 6-well culture plates at a density of 5×10^4 cells per well for 24 h. Then **4-Ir** NPs (0.5 μM) were added into the cell culture medium separately. After incubating for 6 h, the light group were treated with a 635 nm laser (0.6 W cm^{-2}) for 3 min. Laser irradiation was employed to three of the plates (with and without NPs pretreated, 1×10^{-3} m vitamin C pretreated group), whereas the dark control group received nothing. Then using the DMEM solution without FBS the cells were washed. The DMEM solution containing DCFH-DA (10^{-5} mol L^{-1}) was added and incubated for 30 min. The cells were observed as soon as possible by CLSM with excitation at 488 nm.

Live/ dead cell staining assays

HeLa cells were harvested in a logarithmic growth phase and seeded in 96-well plates at a density of 10^4 cells per well for 24 h. The **4-Ir** NPs (0.5 μM) were added into the cell culture medium separately. After incubating for 6 h, the light group was treated with a 635 nm laser (0.6 W cm^{-2}) for 5 min. The incubation at 4 °C and 1×10^{-3} M vitamin C pretreated groups was set as a control. The dark control group received nothing and was incubated for the same time as the control. After staining with calcein-AM/PI for 40 min, phosphate-buffered saline (PBS) was used to wash the cells. Finally, the cells were observed by Nikon C1 Si laser scanning confocal microscopy.

Cellular Uptake

The cellular uptake measurement was investigated by CLSM. Cells harvested in a logarithmic growth phase were seeded in 6-well plates at a density of 5×10^4 cells/well and incubated in DMEM for 24 h. The medium was then replaced by 2 mL of DMEM containing **TPP/1-Ir/4-Ir** NPs (0.5 μM) for different times at 37 °C and further washed 3 times with PBS buffer. For the CLSM, the cells were fixed with 4% paraformaldehyde solution for 10 min. Then, the cells were washed with PBS and observed using confocal laser scanning microscopy with excitation at 555 nm (CLSM, Zeiss LSM 700).

Tumor-bearing mouse model

All animal studies were performed in strict accordance with the NIH guidelines for the care and use of laboratory animals (NIH Publication No. 85-23 Rev. 1985) and were approved by the guidelines of the Committee on Animal Use and Care of the Chinese Academy of Sciences. Male BALB/c mice were purchased from Jilin University, China (6 weeks, 15–20 g). Inoculating the subcutaneous murine 100 μl U14 cells suspension (1×10^4) into the right thigh established the tumor-bearing mouse model.

***In vivo* PDT**

After one week, the mice were intratumorally injected with **4-Ir** NPs (100 μg mL^{-1}, 100 μL), whereas the control group received saline instead. These mice were randomly divided into six groups with four mice in each group: 1) with saline; 2) with saline + Light; 3) **4-Ir** NPs + IT; 4) **4-Ir** NPs + IV; 5) **4-Ir** NPs + IT + Light, 6) **4-Ir** NPs + IV + Light. The mice then received tail intravenous injections and intratumoral

administration. For tumors in the **4-Ir** NPs + IT + Light group, after 1 h the tumor site of the mouse was subjected to 635 nm laser irradiation at intensity 360 J cm^{-2} for 10 min. For tumors in the **4-Ir** NPs + IV + Light group, after 12 h the tumor site of the mouse was subjected to 635 nm laser irradiation at intensity 360 J cm^{-2} for 10 min. The tumor volume and body weight of the mice were measured every 2 days for 14 days.

Histological analysis

The mice were sacrificed at day 14, and major organs and the tumors were collected and fixed in 4% paraformaldehyde. Then they were embedded into paraffin and sliced at a thickness of 5 μm. Slices were stained with hematoxylin and eosin (H&E) and imaged by optical microscopy.

2. General information and methods

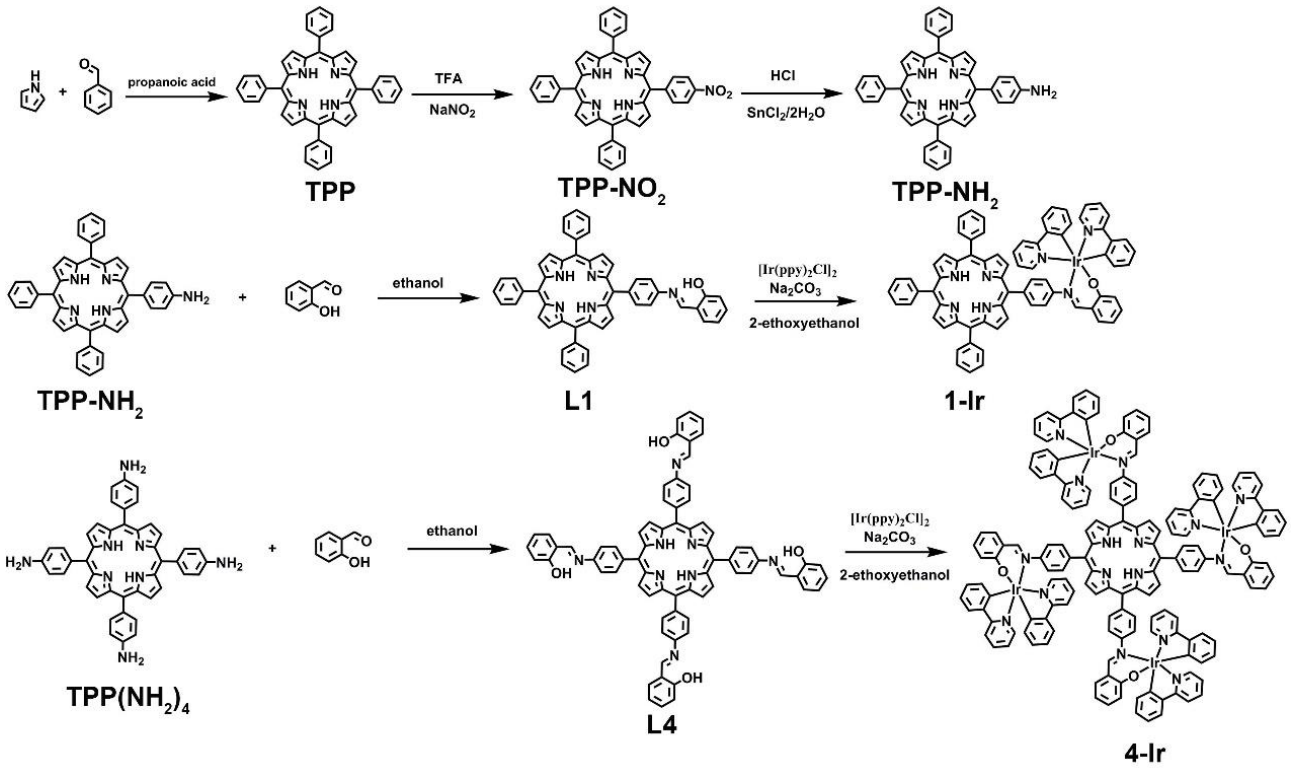

Scheme S1. Synthetic routes to **TPP**, **1-Ir** and **4-Ir**.

Synthesis and Characterization of **TPP**: Benzaldehyde (5.30 g, 50 mmol) in propanoic acid (60 ml) was stirred under argon. The solution was heated to 135 °C and pyrrole (3.35 g, 50 mmol) was slowly added. The mixture was refluxed for another 7 h. Then, it was stored at -20 °C for 12 h. The precipitate was filtered and washed with ethanol. A violet solid was obtained (2.92 g, 38% yield). ^{1}H NMR (500 MHz, $CDCl_3$, δ [ppm]): 8.84 (s, 8H, ArH), 8.22 (d, J = 6.0 Hz, 8H, ArH), 7.73-7.79 (m, 12H, ArH), -2.77 (s, 2H, Inner pyrroleH). ^{13}C NMR (151 MHz, $CDCl_3$, δ [ppm]): 142.2, 134.6, 127.7, 126.7, 120.2. MS: (ESI-TOF) [m/z]: 615.2 (calcd: 614.2). Anal. Calcd. for $C_{44}H_{30}N_4$: C 85.97, H 4.92, N 9.11. Found C 85.97, H 4.91, N 9.12.

Synthesis and Characterization of **TPP-NO_2**: **TPP** (0.10 g, 0.163 mmol) and sodium nitrite (0.20 g, 0.29 mmol) in TFA (10 ml) were stirred at room temperature for 3 min. Then, water (10 ml) was added to the solution and stirred for 2 h. The reaction mixture was neutralized with ammonia solution to ca. pH = 7.0, the solution was extracted with dichloromethane (250 ml) and washed with water (100 ml). Then, the filtrate was removed by evaporation, the residue was purified by column chromatography with petroleum ether / dichloromethane / (3:2 v/v) as eluent. A violet solid was obtained (0.052 g, 49% yield). ^{1}H NMR (500 MHz, $CDCl_3$, δ [ppm]): 8.84-8.89 (m, 6H, ArH), 8.74 (d, J = 6.0 Hz, 2H, ArH), 8.64 (d, J = 4.5 Hz, 2H, ArH), 8.40 (d, J = 8.0 Hz, 2H, ArH), 8.21 (d, J = 7.5 Hz, 6H, ArH), 7.74-7.80 (m, 9H, ArH), -2.78 (s, 2H, Inner pyrroleH).

Synthesis and Characterization of **TPP-NH_2**: **TPP-NO_2** (2.50 g, 3.79 mmol) in conc. HCl solution (80 ml) was stirred under argon. The solution was heated to 65 °C and $SnCl_2 \cdot 2H_2O$ (2.60 g, 11.5 mmol) was slowly added. The mixture was refluxed for another 12 h. After cooling to room temperature, water (300 ml) was added to the solution and then neutralized to around pH = 8.0 with ammonia solution. The solution was extracted with dichloromethane (250 ml) and washed with water (100 ml). Then, the filtrate was removed by evaporation, the residue was purified by column chromatography with petroleum ether / dichloromethane / (1:1 v/v) as eluent. A violet solid was obtained (1.79 g, 75% yield). ^{1}H NMR (500

MHz, $CDCl_3$, δ [ppm]): 8.94 (d, J = 5.0 Hz, 2H, ArH), 8.83 (s, 6H, ArH), 8.22 (d, J = 6.0 Hz, 6H, ArH), 7.99 (t, J = 6.0 Hz, 2H, ArH), 7.73-7.77 (m, 9H, ArH), 7.06 (d, J = 7.5 Hz, 2H, ArH), 4.01 (s, 2H, NH) -2.76 (S, 2H, Inner pyrroleH).

Synthesis and Characterization of **L1**: **TPP-NH_2** (0.629 g, 1.0 mmol) and salicylaldehyde (0.146 g, 1.2 mmol) in ethanol (60 ml) were stirred at 79 °C for 8 h. After cooling to room temperature, the precipitate was filtered and recrystallized from ethanol. A violet solid was obtained (0.60 g, 82% yield). ^{1}H NMR (500 MHz, $CDCl_3$, δ [ppm]): 13.44 (s, 1H, OH), 9.00 (s, 1H, CH), 8.85-8.89 (m, 8H, ArH), 8.28 (d, J = 8.0 Hz, 2H, ArH), 8.22 (t, J = 6.0 Hz, 6H, ArH), 7.74-7.80 (m, 9H, ArH), 7.69 (d, J = 8.5 Hz, 2H, ArH), 7.56 (d, J = 6.0 Hz, 1H, ArH), 7.48 (t, J = 6.5 Hz, 1H, ArH), 7.14 (d, J = 7.5 Hz, 1H, ArH), 7.05 (t, J = 6.0 Hz, 1H, ArH), -2.76 (s, 2H, Inner pyrroleH).

Synthesis and Characterization of **L4**: **TPP(NH_2)$_4$** (0.629 g, 1.0 mmol) and salicylaldehyde (0.584 g, 4.8 mmol) in ethanol (60 ml) were stirred at 79 °C for 8 h. After cooling to room temperature, the precipitate was filtered and recrystallized from ethanol. A violet solid was obtained (0.97 g, 89% yield). ^{1}H NMR (500 MHz, $CDCl_3$, δ [ppm]): 13.44 (s, 4H, OH), 9.01 (s, 4H, CH), 8.94 (s, 8H, ArH), 8.30 (d, J = 8.0 Hz, 8H, ArH), 7.72 (d, J = 6.0 Hz, 8H, ArH), 7.57 (d, J = 4.5 Hz, 4H, ArH), 7.47 (t, J = 8.5 Hz, 4H, ArH), 7.14 (d, J = 7.5 Hz, 4H, ArH), 7.05 (t, J = 7.5 Hz, 4H, ArH), -2.71 (s, 2H, Inner pyrroleH).

Synthesis and Characterization of **1-Ir**: A yellow suspension of the dichloro-bridged diiridium complex $[Ir(ppy)_2Cl]_2$ (0.107 g, 0.1 mmol), **L1** (0.146 g, 0.2 mmol) and Na_2CO_3 (0.349 g, 3.2 mmol) in 2-ethoxyethanol (60 ml) was stirred at 120 °C for 8 h under argon. After cooling to room temperature, the solution was extracted with dichloromethane (250 ml) and washed with water (100 ml). Then, the filtrate was removed by evaporation, the residue was purified by column chromatography with dichloromethane / acetone (30:1 v/v) as eluent. A violet solid was obtained (0.199 g, 81% yield). ^{1}H NMR (500 MHz, $CDCl_3$, δ [ppm]): 9.11 (d, J = 6.0 Hz, 1H, ArH), 9.08 (d, J = 6.5 Hz, 1H, ArH), 8.83 (s, 6H, ArH), 8.64

(d, J = 4.5 Hz, 2H, ArH), 8.49 (s, 1H, CH), 8.22 (t, J = 7.5 Hz, 6H, ArH), 7.94 (d, J = 8.0 Hz, 1H, ArH), 7.73-7.84 (m, 12H, ArH), 7.61-7.64 (m, 3H, ArH), 7.54 (t, J = 6.5 Hz, 1H, ArH), 7.32 (t, J = 4.5 Hz, 2H, ArH), 7.22 (t, J = 5.0 Hz, 1H, ArH), 7.14 (t, J = 8.5 Hz, 1H, ArH), 6.90 (t, J = 6.5 Hz, 1H, ArH), 6.86 (t, J = 4.5 Hz, 1H, ArH), 6.77-6.81 (m, 2H, ArH), 6.68 (t, J = 5.0 Hz, 1H, ArH), 6.60 (d, J = 4.5 Hz, 2H, ArH), 6.49 (t, J = 8.5 Hz, 1H, ArH), 6.38-6.42 (m, 2H, ArH), -3.85 (s, 2H, Inner pyrroleH). ^{13}C NMR (151 MHz, $CDCl_3$, δ [ppm]): 169.0, 168.8, 167.1, 162.0, 152.4, 152.2, 150.6, 149.4, 148.7, 144.6, 144.5, 142.22, 142.16, 138.7, 137.0, 136.8, 135.5, 134.6, 134.4, 133.8, 133.7, 132.6, 131.0, 130.9, 129.5, 129.4, 128.9, 128.8, 127.79, 127.76, 126.8, 126.7, 125.1, 124.0, 123.9, 121.7, 121.5, 121.4, 120.7, 120.5, 120.2, 120.1, 119.5, 119.1, 118.1, 113.6. MS: (MALDI-TOF) [m/z]: 1233.4 (calcd: 1233.4). Anal. Calcd. for $C_{73}H_{50}IrN_7O$: C 71.08, H 4.09, N 7.95. Found C 71.07, H 4.09, N 7.96.

Synthesis and Characterization of **4-Ir**: A yellow suspension of the dichloro-bridged diiridium complex $[Ir(ppy)_2Cl]_2$ (0.214 g, 0.2 mmol), **L4** (0.109 g, 0.1 mmol) and Na_2CO_3 (0.349 g, 3.2 mmol) in 2-ethoxyethanol (60 ml) was stirred at 120 °C for 8 h under argon. After cooling to room temperature, the solution was extracted with dichloromethane (250 ml) and washed with water (100 ml). Then, the filtrate was removed by evaporation, the residue was purified by column chromatography with dichloromethane / acetone (10:1 v/v) as eluent. A violet solid was obtained (0.23 g, 73% yield). ^{1}H NMR (500 MHz, $CDCl_3$, δ [ppm]): 9.13 (d, J = 6.0 Hz, 4H, ArH), 9.10 (d, J = 6.0 Hz, 4H, ArH), 8.63 (s, 6H, ArH), 8.53 (s, 4H, CH), 7.95 (d, J = 7.5 Hz, 4H, ArH), 7.85-7.89 (m, 4H, ArH), 7.76 (t, J = 8.0 Hz, 8H, ArH), 7.56-7.65 (m, 16H, ArH), 7.30-7.34 (m, 10H, ArH), 7.23 (t, J = 6.5 Hz, 4H, ArH), 7.14 (t, J = 4.5 Hz, 4H, ArH), 6.85-6.92 (m, 8H, ArH), 6.78-6.81 (m, 8H, ArH), 6.70 (t, J = 6.0 Hz, 4H, ArH), 6.64 (d, J = 7.0 Hz, 8H, ArH), 6.49 (t, J = 8.5 Hz, 4H, ArH), 6.43-6.45 (m, 4H, ArH), 6.38 (d, J = 5.0 Hz, 4H, ArH), -3.03 (s, 2H, Inner pyrroleH). ^{13}C NMR (151 MHz, $CDCl_3$, δ [ppm]): 168.6, 168.26, 166.32, 162.7, 153.1, 152.8, 151.1, 150.2, 148.1, 145.6, 145.2, 138.5, 137.9, 137.0, 134.6, 133.7, 132.7, 130.1, 128.8, 124.3, 124.0, 123.3, 122.7, 122.0, 121.0, 120.5, 119.7, 119.0, 113.7. MS: (MALDI-TOF) [m/z]: 3090.7 (calcd: 3090.7). Anal. Calcd. for $C_{160}H_{110}Ir_4N_{16}O_4$: C 62.20, H 3.59, N 7.25. Found C 62.30, H 3.58, N 7.25.

3. Supplementary Figures

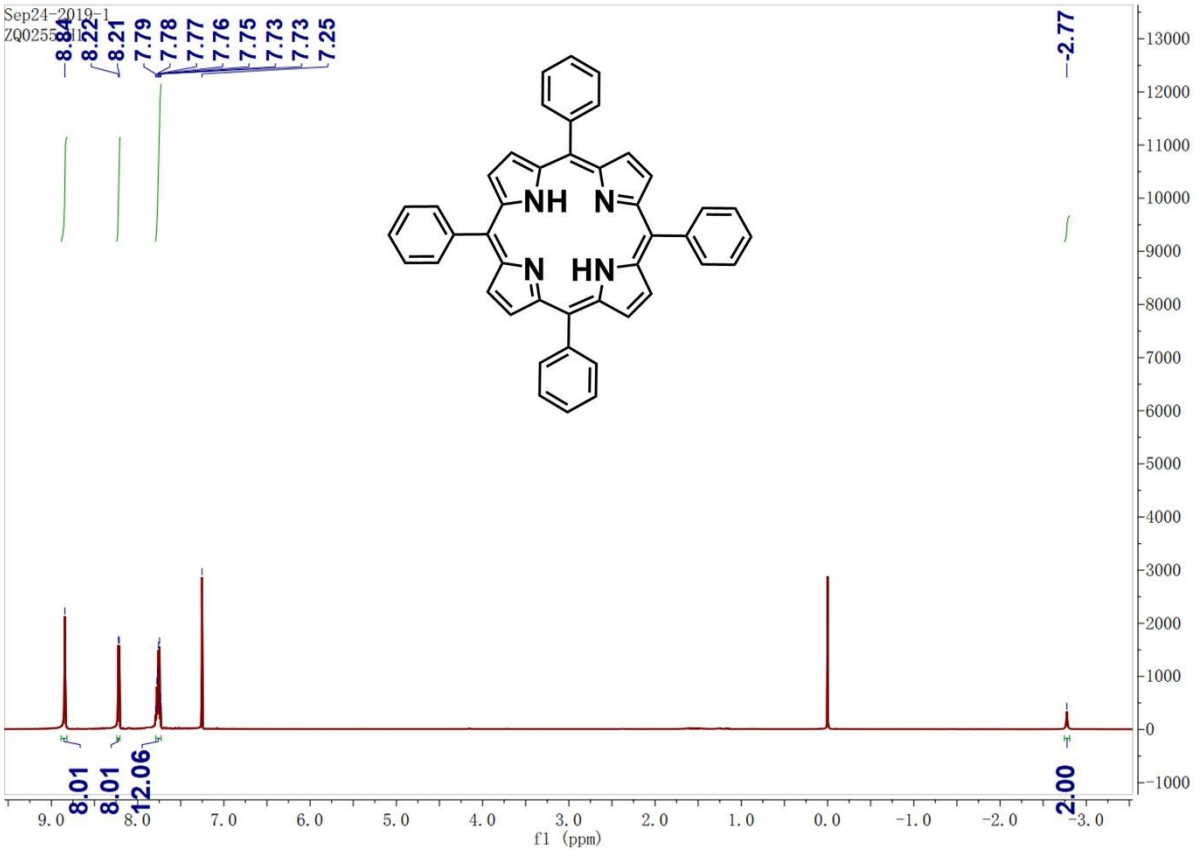

Fig. S1 ^{1}H NMR spectrum of **TPP** in $CDCl_3$.

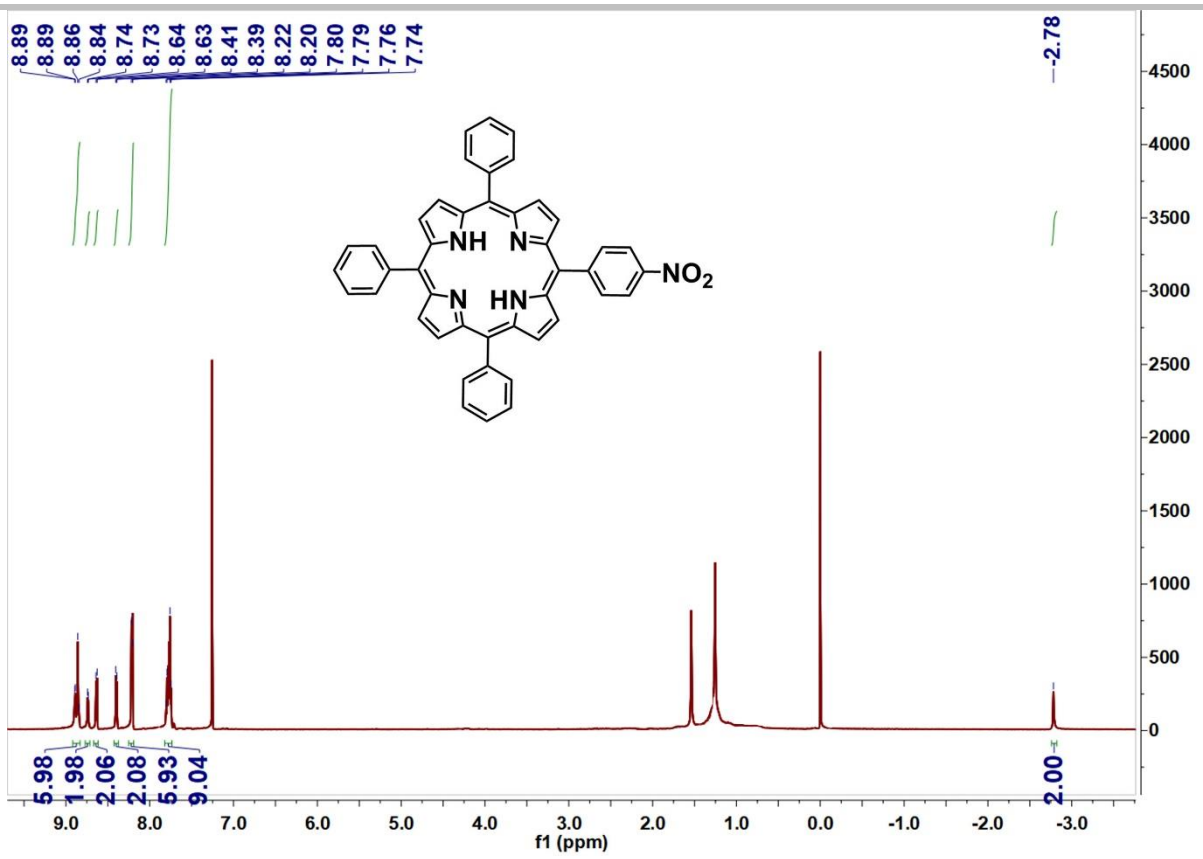

Fig. S2 ^{1}H NMR spectrum of **TPP-NO$_2$** in $CDCl_3$.

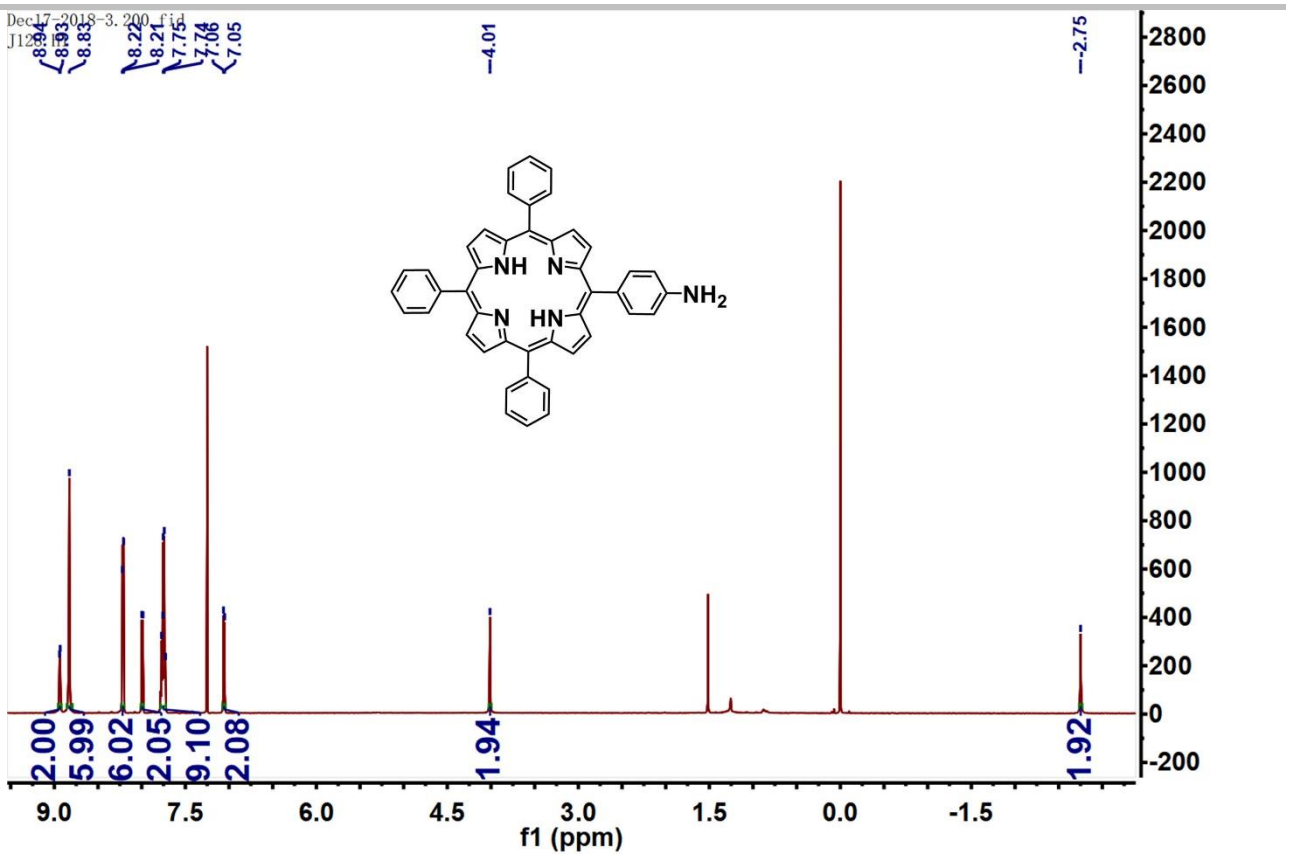

Fig. S3 ^{1}H NMR spectrum of **TPP-NH$_2$** in $CDCl_3$.

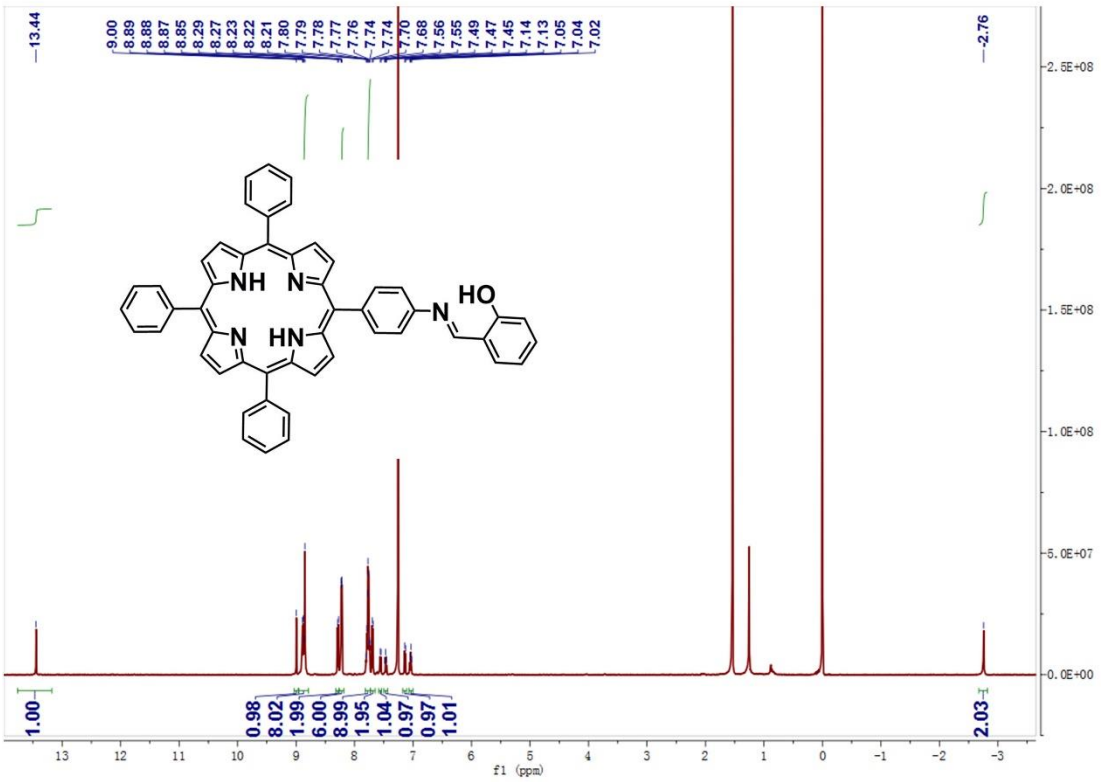

Fig. S4 ^{1}H NMR spectrum of **L1** in $CDCl_3$.

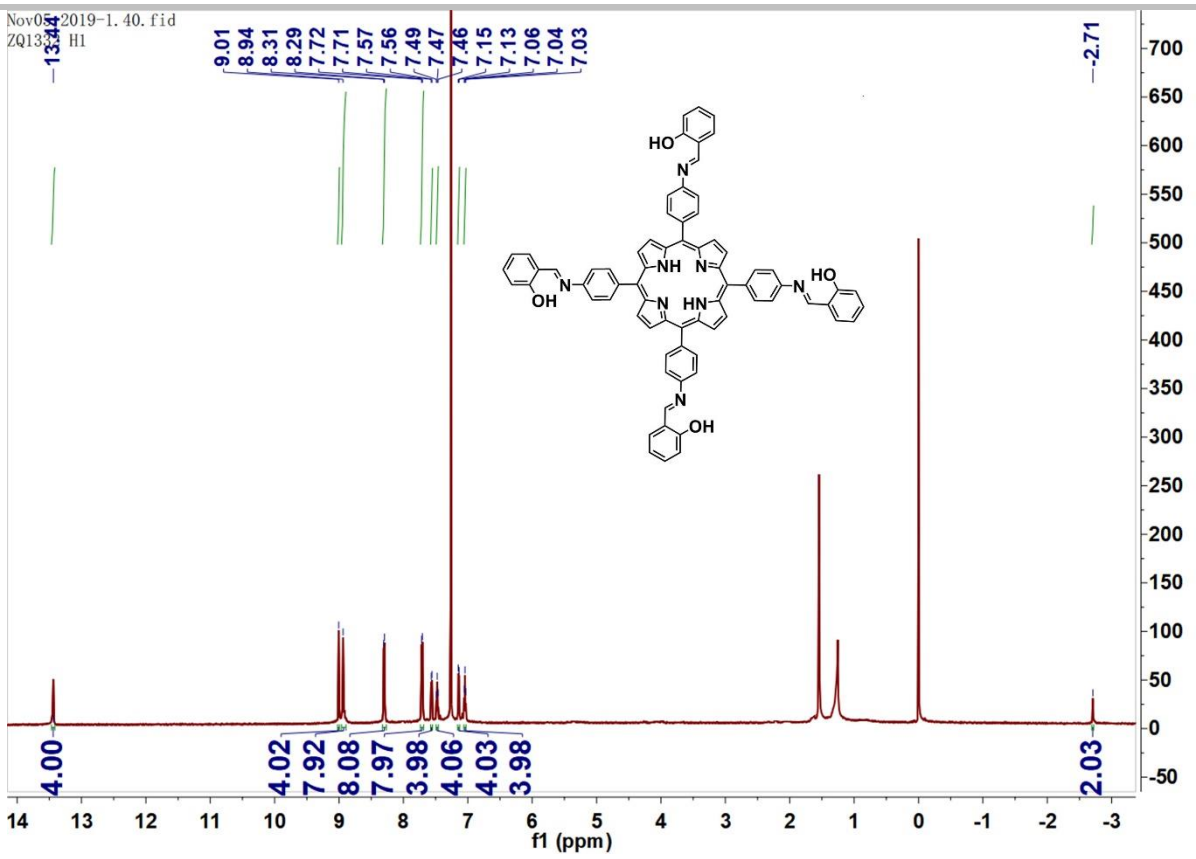

Fig. S5 ^{1}H NMR spectrum of **L4** in $CDCl_3$.

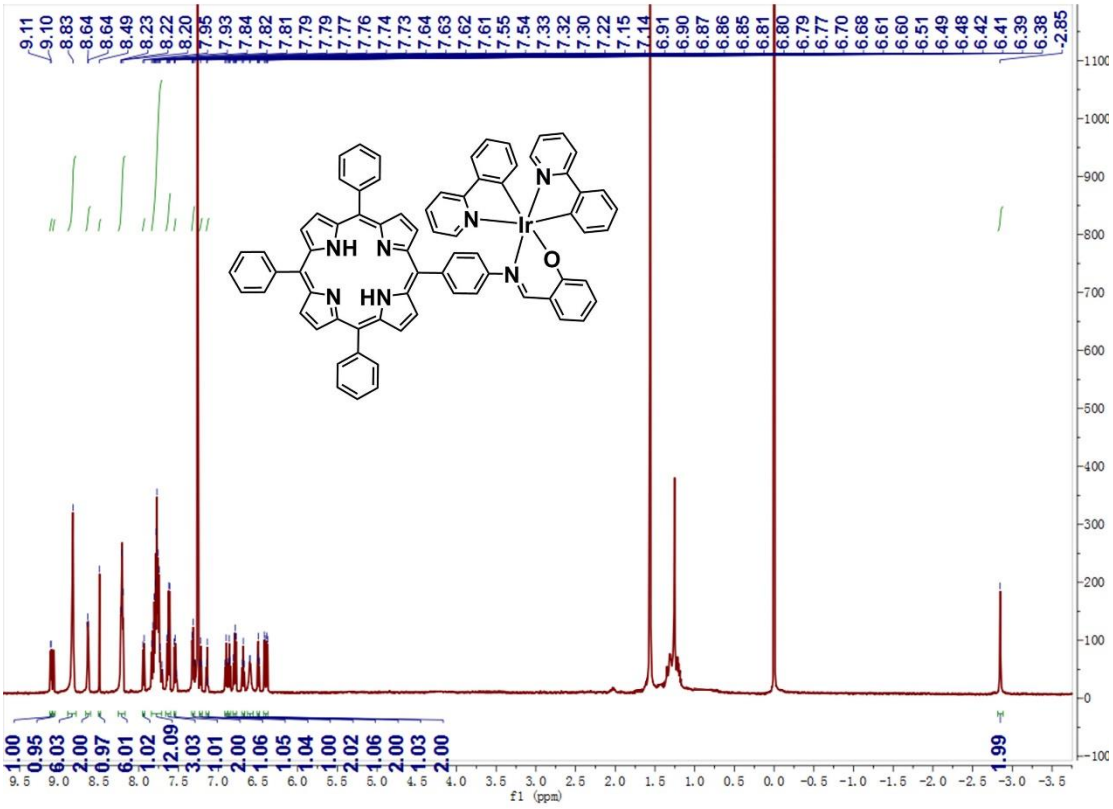

Fig. S6 ^{1}H NMR spectrum of **1-Ir** in $CDCl_3$.

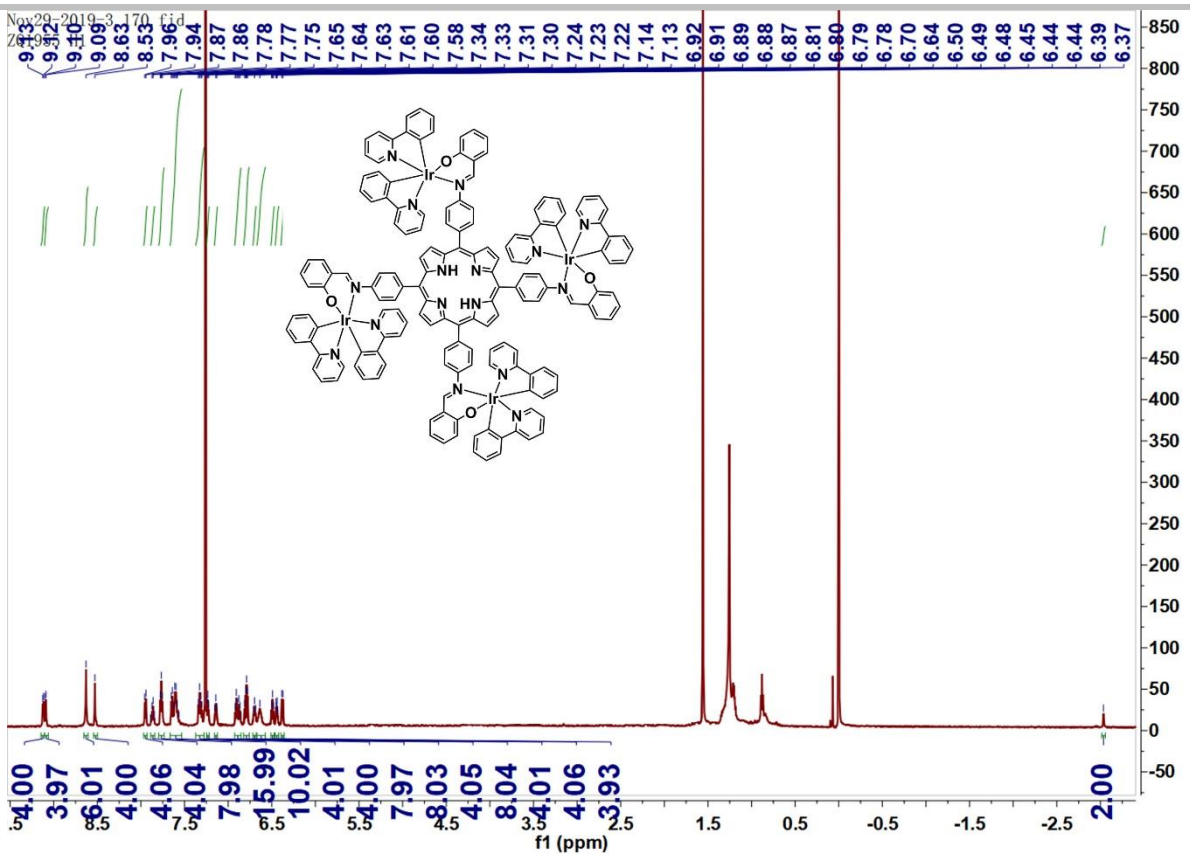

Fig. S7 ^{1}H NMR spectrum of **4-Ir** in $CDCl_3$.

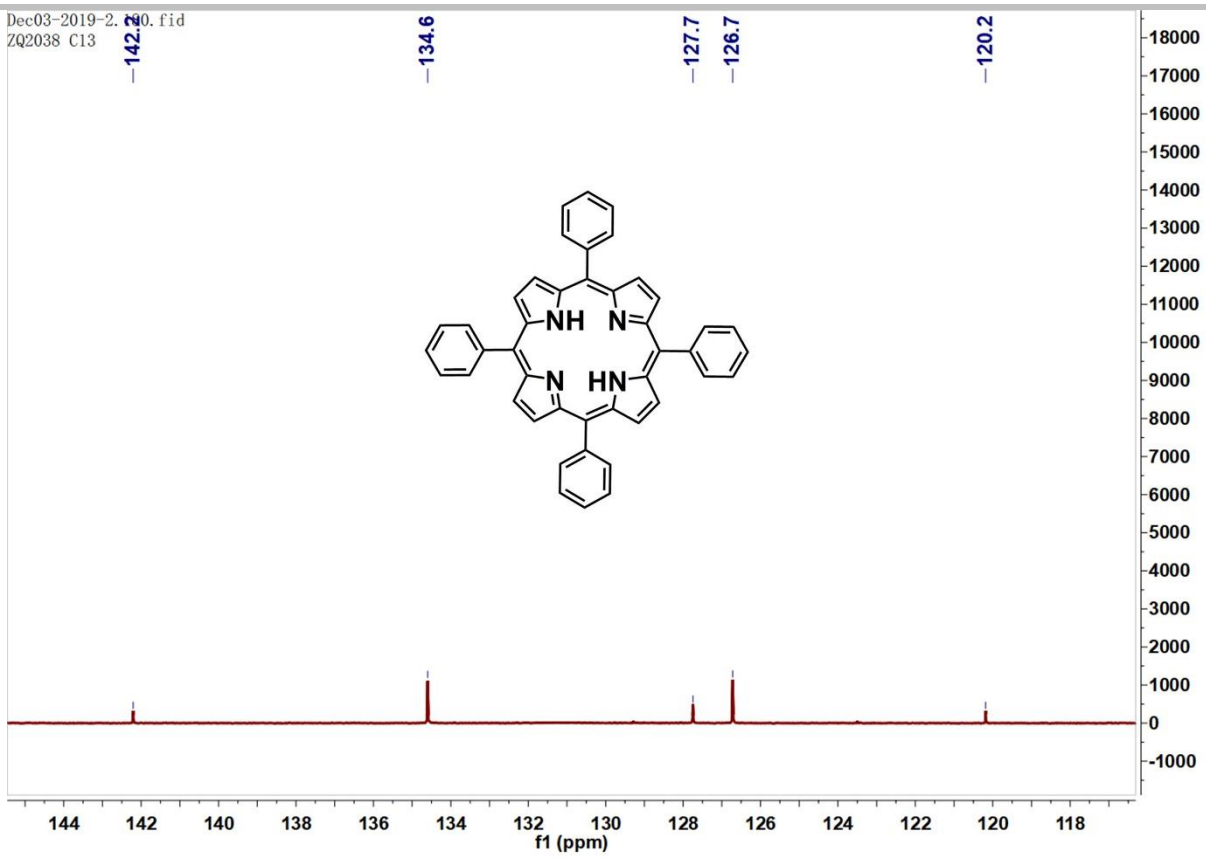

Fig. S8 ^{13}C NMR spectrum of **TPP** in $CDCl_3$.

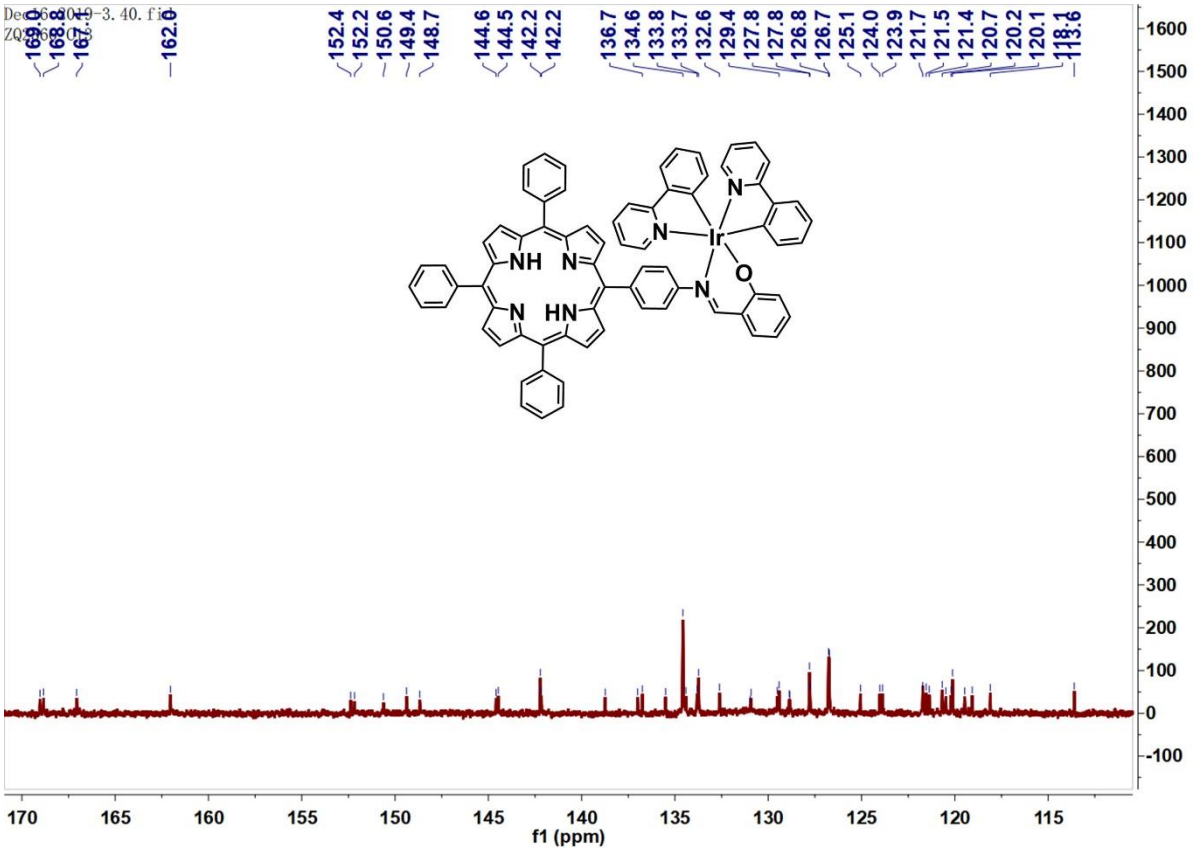

Fig. S9 ^{13}C NMR spectrum of **1-Ir** in $CDCl_3$.

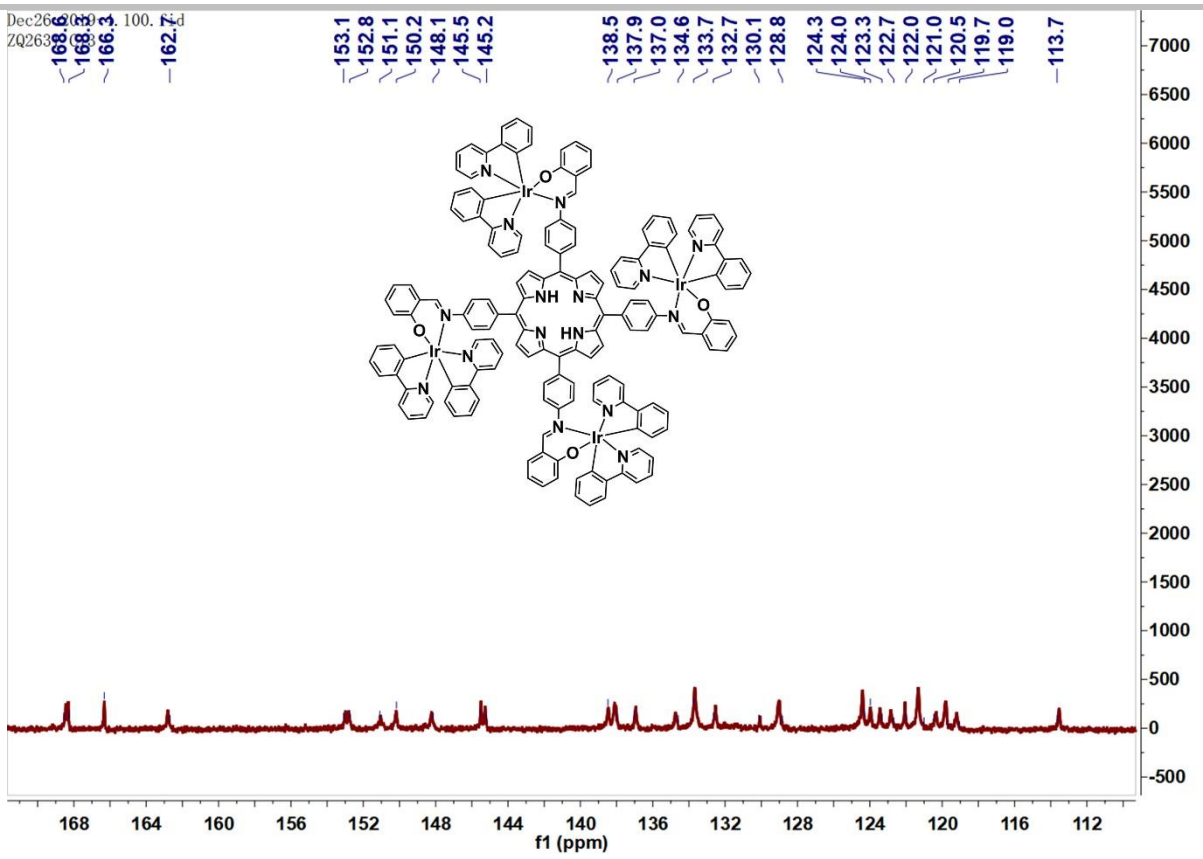

Fig. S10 ^{13}C NMR spectrum of **4-Ir** in $CDCl_3$.

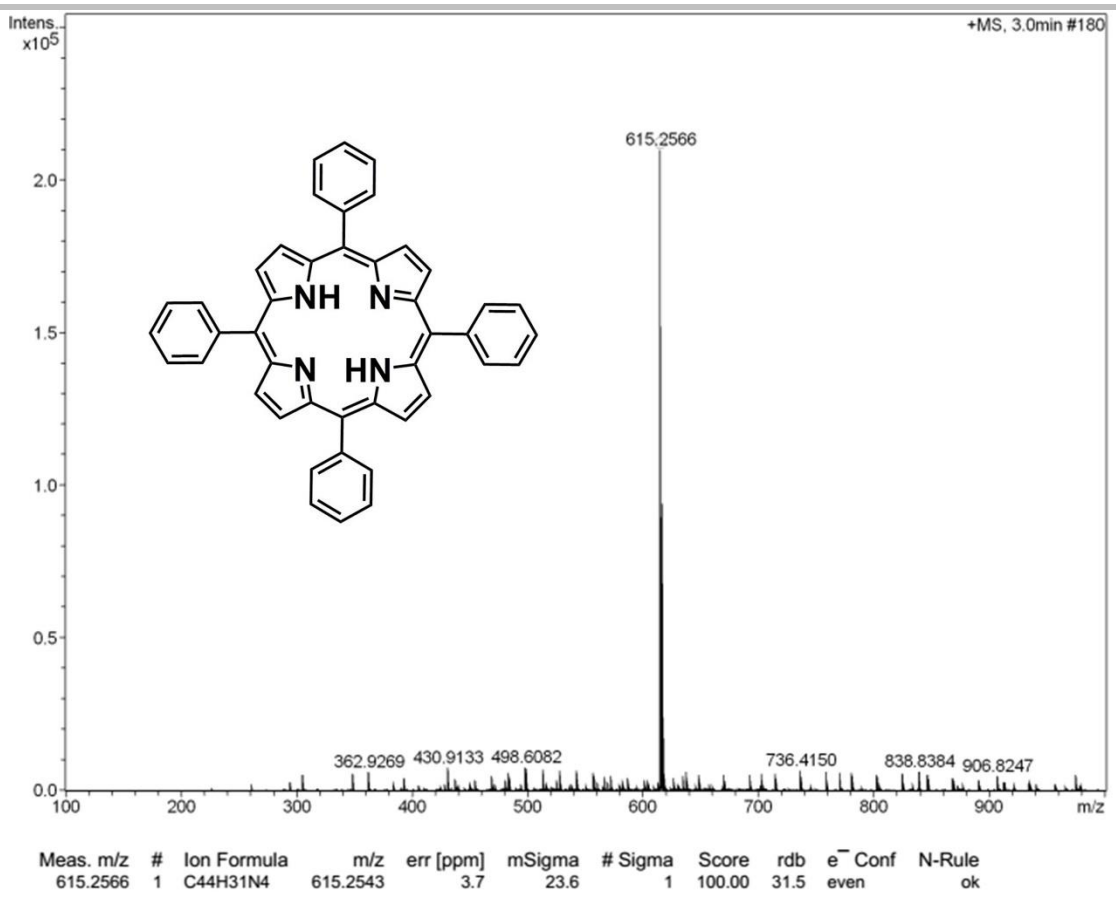

Fig. S11 ESI mass spectrum of **TPP**.

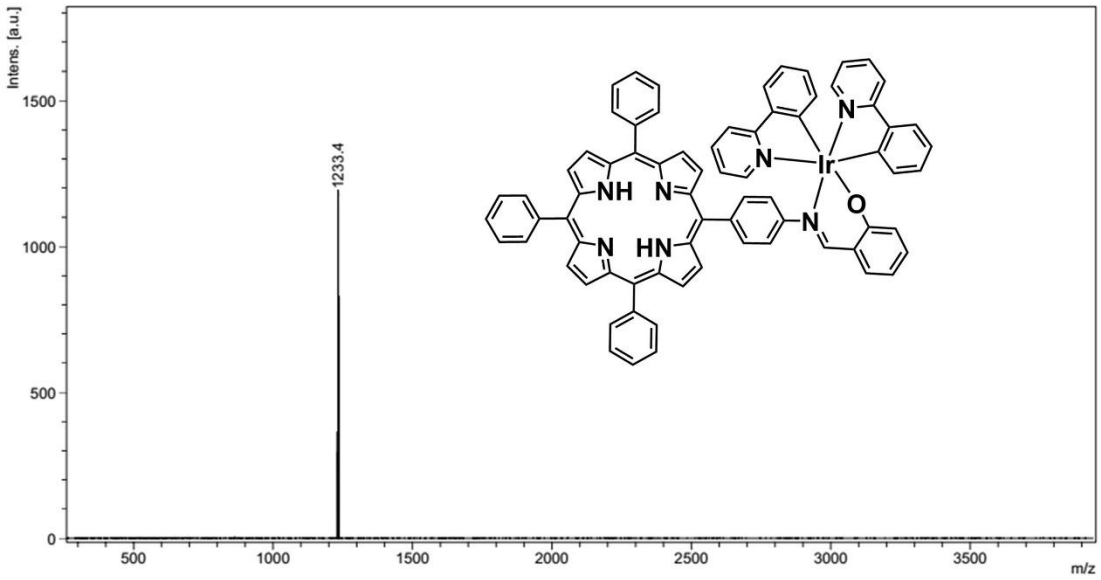

Fig. S12 MALDI-TOF mass spectrum of **1-Ir**.

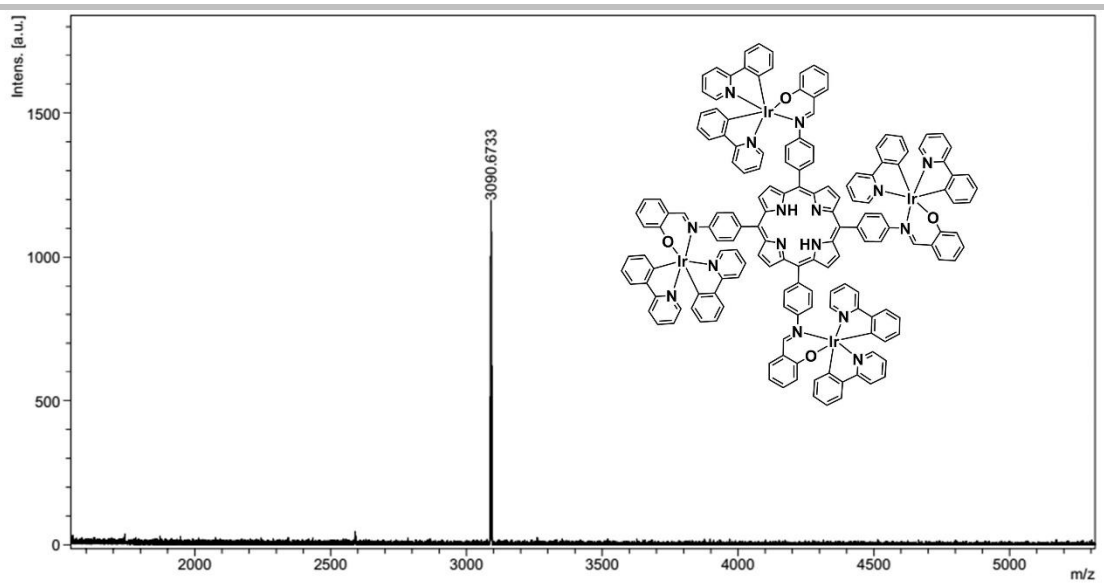

Fig. S13 MALDI-TOF mass spectrum of **4-Ir**.

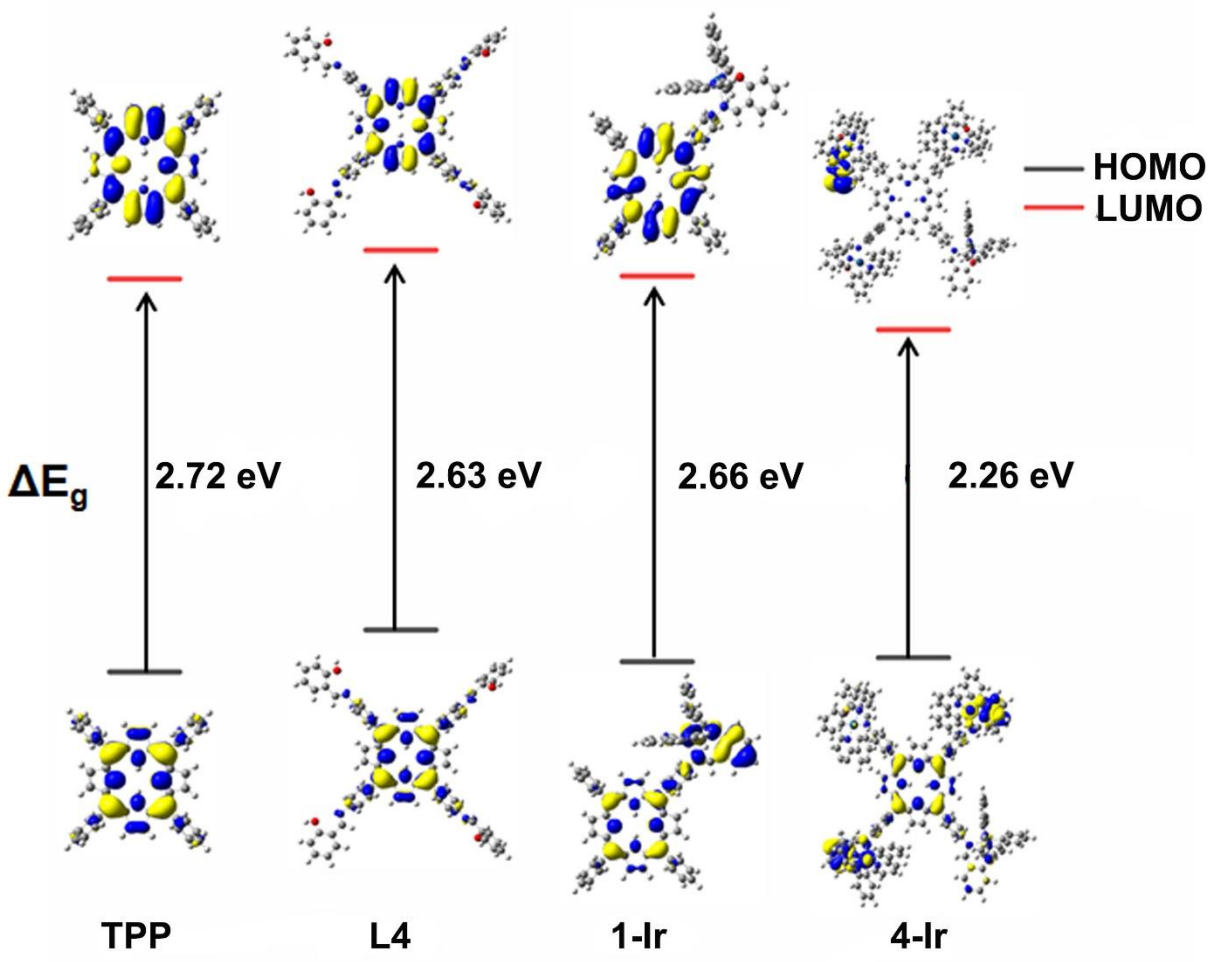

Fig. S14 Calculated HOMO, LUMO energy levels of PSs.

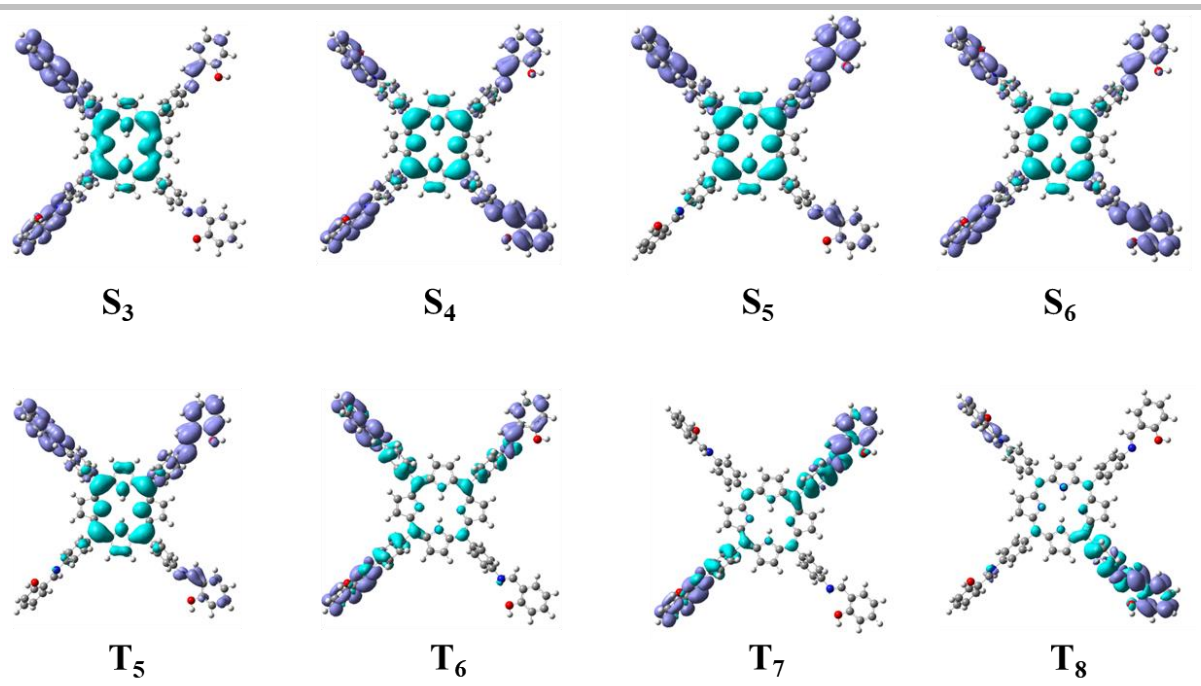

Fig. S15 The charge density distributions of the excited states in **L4**.

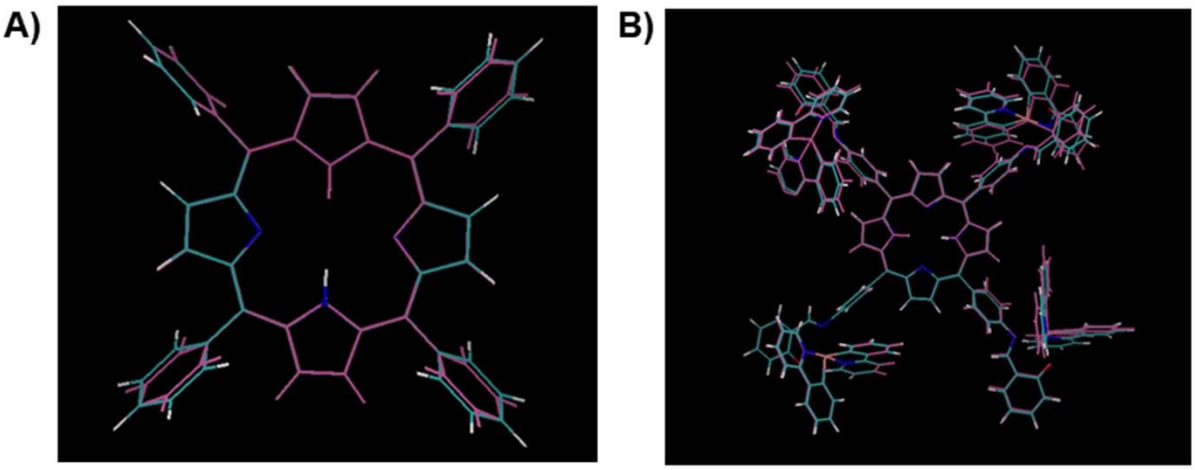

Fig. S16 The comparison of the geometrical structures at S_0 and T_1 states for A) **TPP** and B) **4-Ir**. Their root mean square deviation (RMSD) is 0.16 Å and 0.46 Å, respectively.

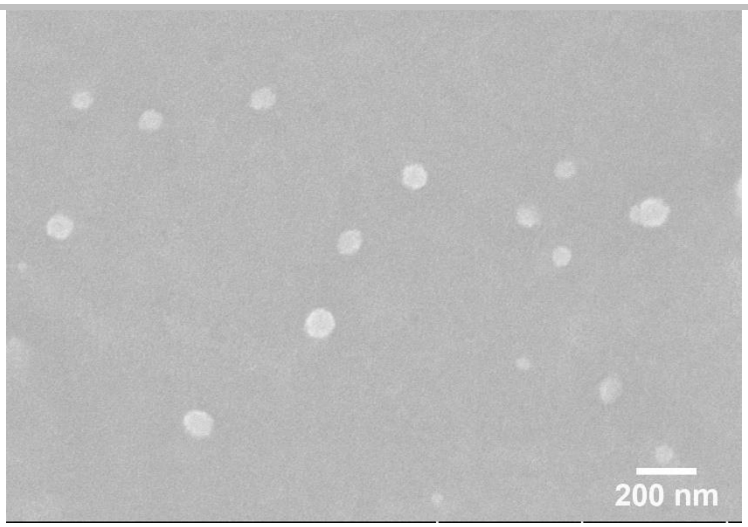

Fig. S17 SEM images of **4-Ir** NPs.

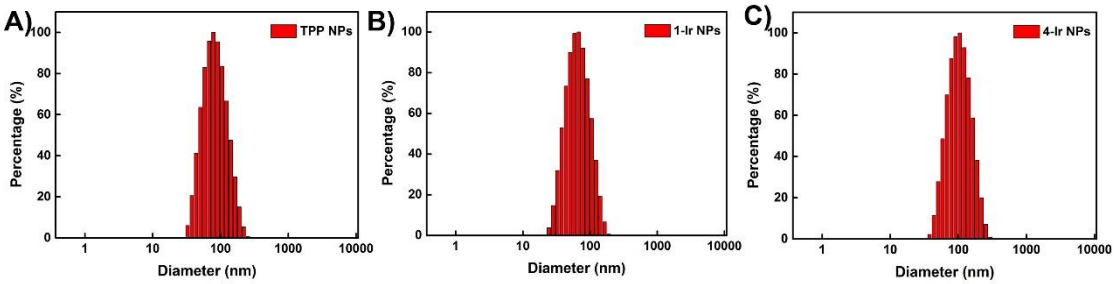

Fig. S18 Dynamic light scattering results of A) **TPP** NPs, B) **1-Ir** NPs and C) **4-Ir** NPs in water.

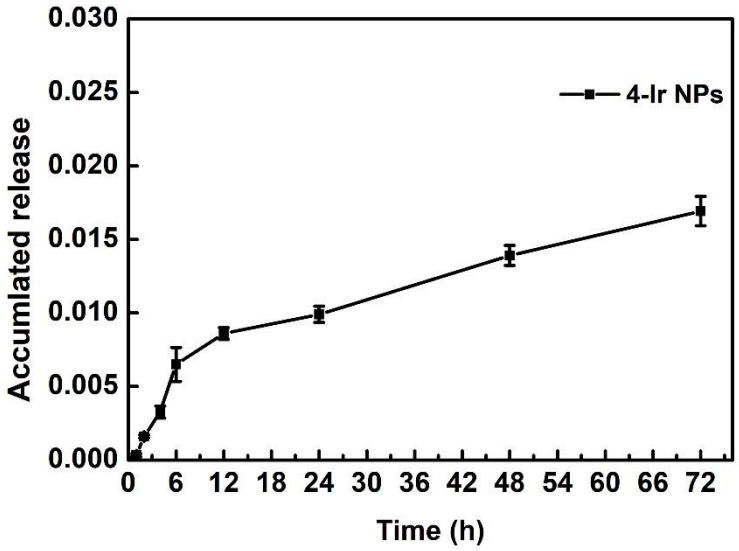

Fig. S19 Time course of release profiles of **4-Ir** from **4-Ir** NPs in water.

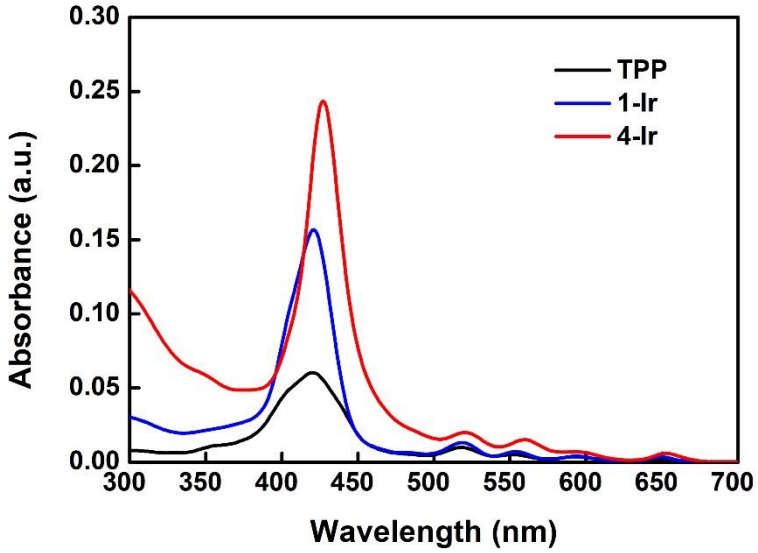

Fig. S20 UV–vis absorption spectra of PSs in tetrahydrofuran (1×10^{-5} M).

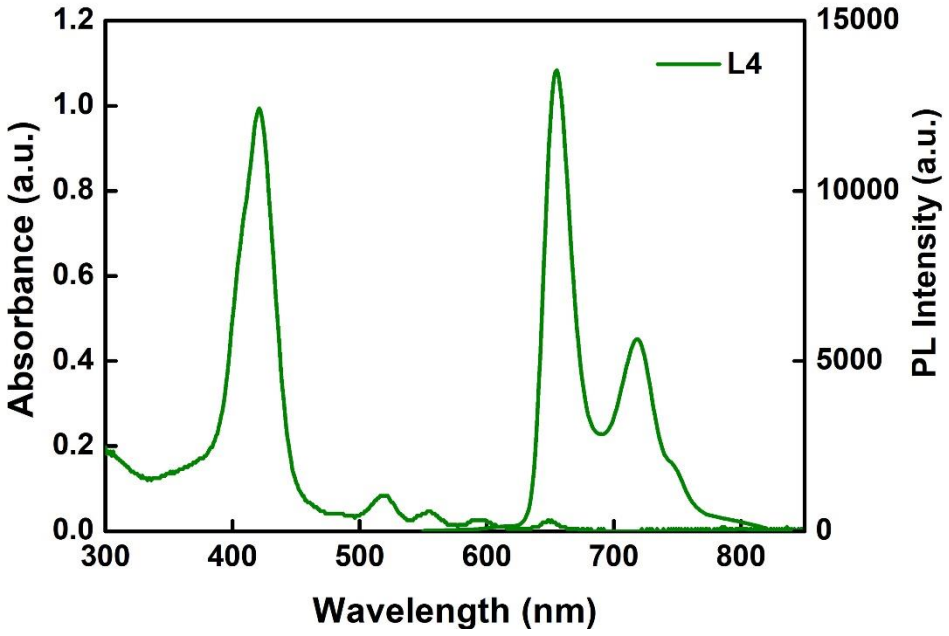

Fig. S21 UV–vis absorption and photoluminescence spectra of **L4** in tetrahydrofuran (1×10^{-5} M).

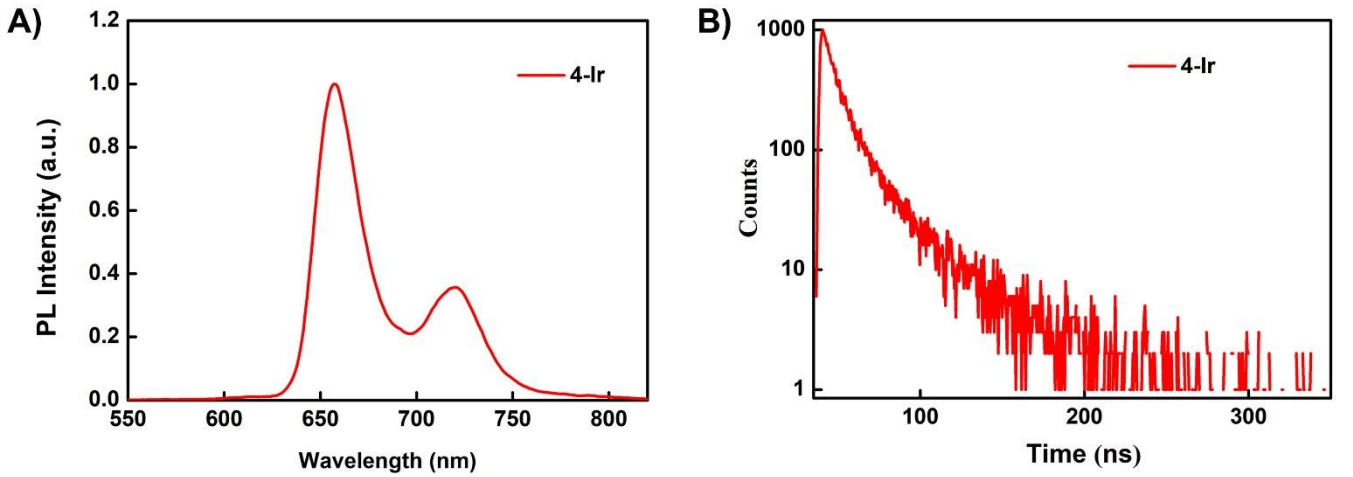

Fig. S22 A) The emission spectrum of **4-Ir** (1×10^{-5} M) in THF/water (v:v) = 1/9; B) emission decay of **4-Ir** (1×10^{-5} M) in THF/water (v:v) = 1/9 at 77 K.

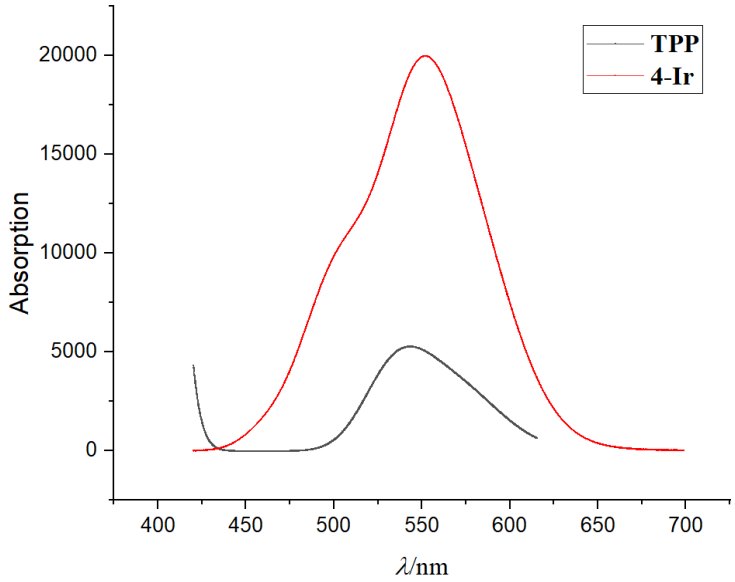

Fig. S23 The simulated absorption spectra for **TPP** and **4-Ir** in the long-wavelength region by TDDFT/B3LYP method.

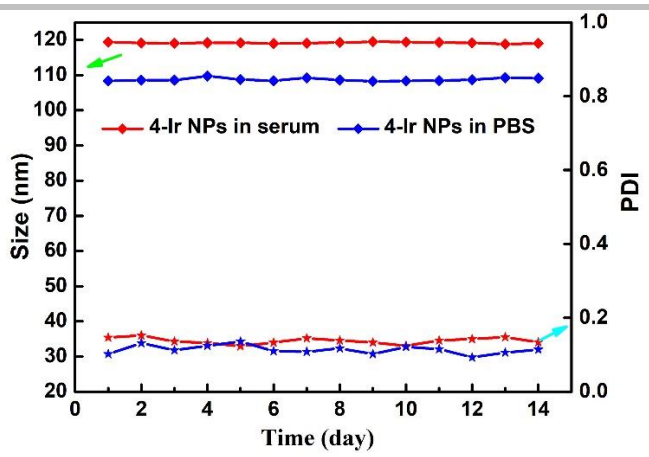

Fig. S24 Stability of size distribution of **4-Ir** in serum and PBS during 14 days.

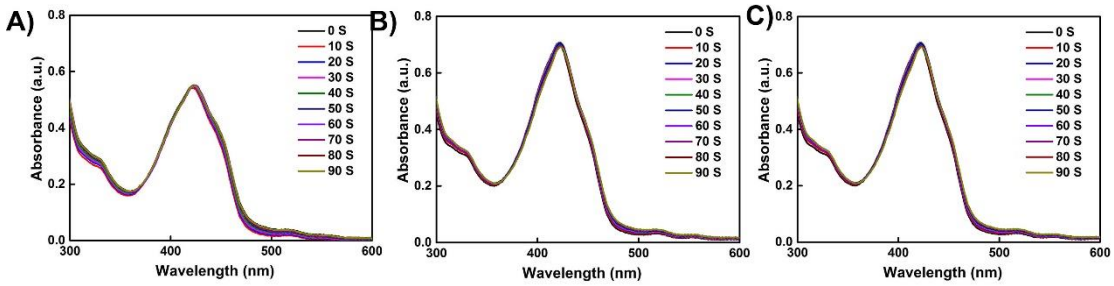

Fig. S25 UV-vis absorption spectra of DPBF (1.5×10^{-6} M) in the presence of A) **TPP** NPs, B) **1-Ir** NPs and C) **4-Ir** NPs (1×10^{-6} M) at different times.

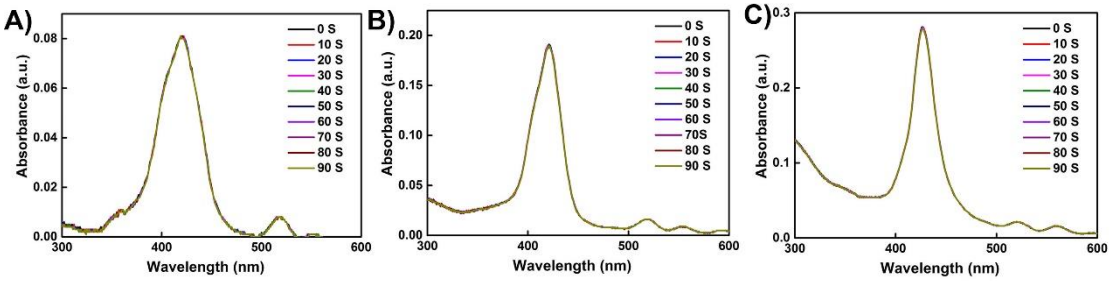

Fig. S26 UV-vis absorption spectra of A) **TPP** NPs, B) **1-Ir** NPs and C) **4-Ir** NPs (1×10^{-6} M) for different times under irradiation (635 nm, 0.4 W cm^{-2}).

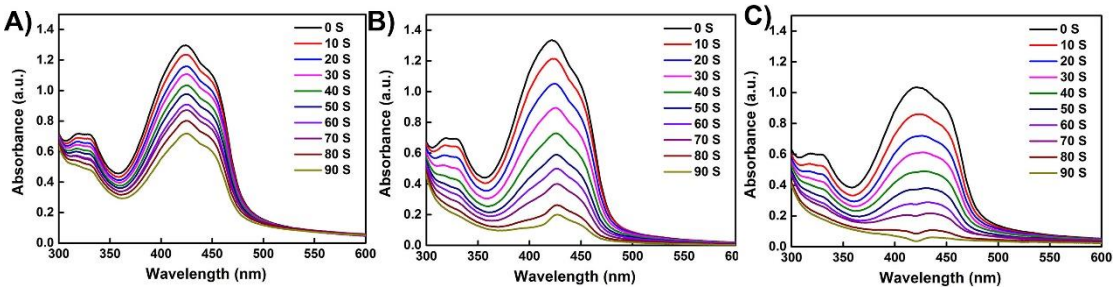

Fig. S27 UV-vis absorption spectra of DPBF (1.5×10^{-5} M) in the presence of A) **TPP** NPs, B) **1-Ir** NPs and C) **4-Ir** NPs (1×10^{-6} M) for different times under irradiation (635 nm, 0.4 W cm^{-2}).

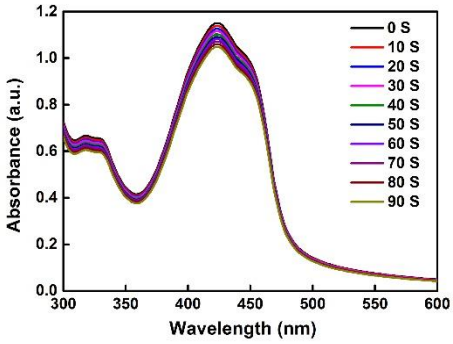

Fig. S28 UV-vis absorption spectra of DPBF (1.5×10^{-5} M) for different times under irradiation (635 nm, 0.4 W cm^{-2}).

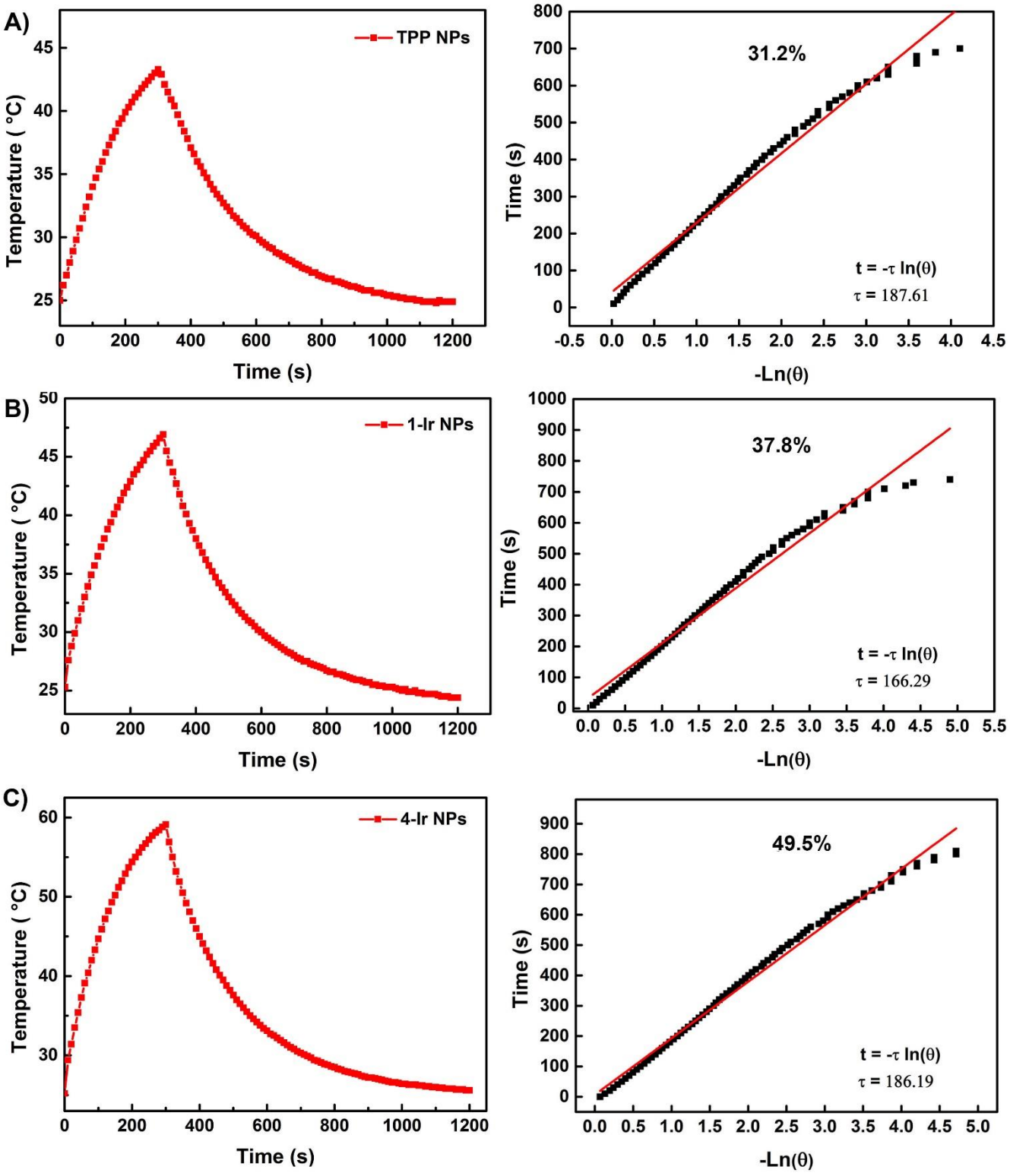

Fig. S29 Photothermal effect under irradiation of a 635 nm laser (0.8 W cm^{-2}) and plot of cooling time versus negative natural logarithm of A) **TPP** NPs, B) **1-Ir** NPs and C) **4-Ir** NPs.

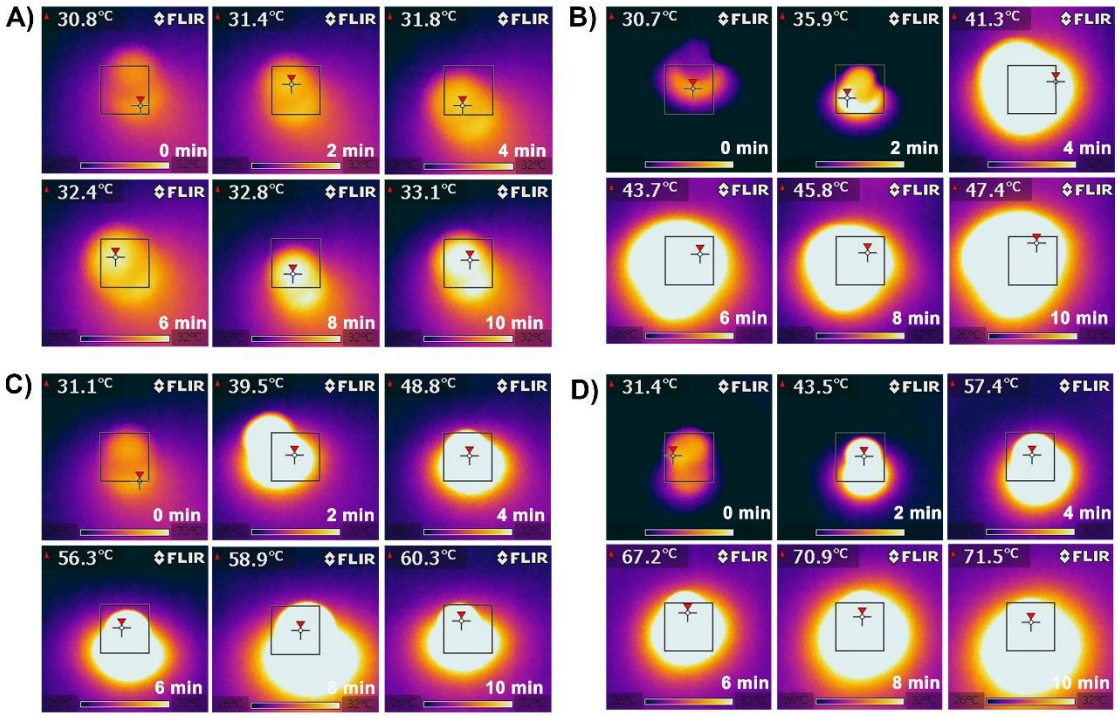

Fig. S30 Infrared thermal images: A) water, B) **TPP** NPs, C) **1-Ir** NPs and D) **4-Ir** NPs, respectively, exposed to 635 nm laser (0.8 W cm^{-2}) recorded at different time intervals.

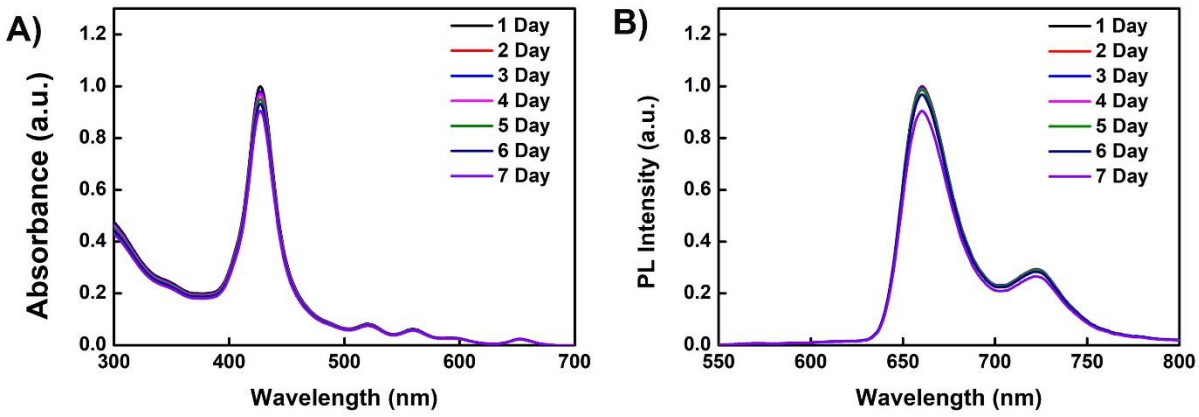

Fig. S31 A) The absorbance intensity and B) the PL intensity of **4-Ir** NPs (1×10^{-6} M) after irradiation with a 635 nm laser (0.8 W cm^{-2}, 5 min) for seven days.

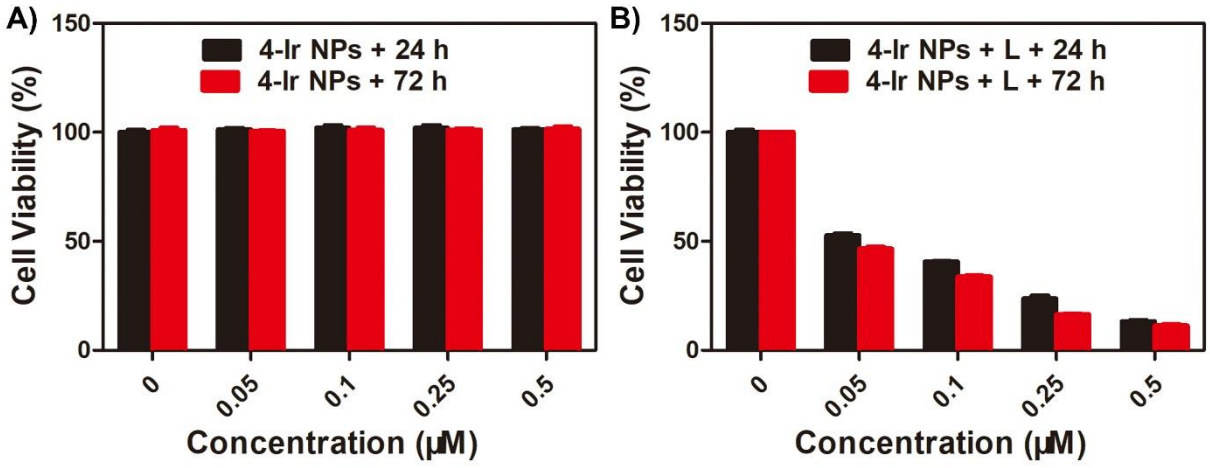

Fig. S32 Cell viability of **4-Ir** NPs against HeLa cells: A) in the dark and B) under light (635 nm, 0.6 W cm^{-2}, 5 min).

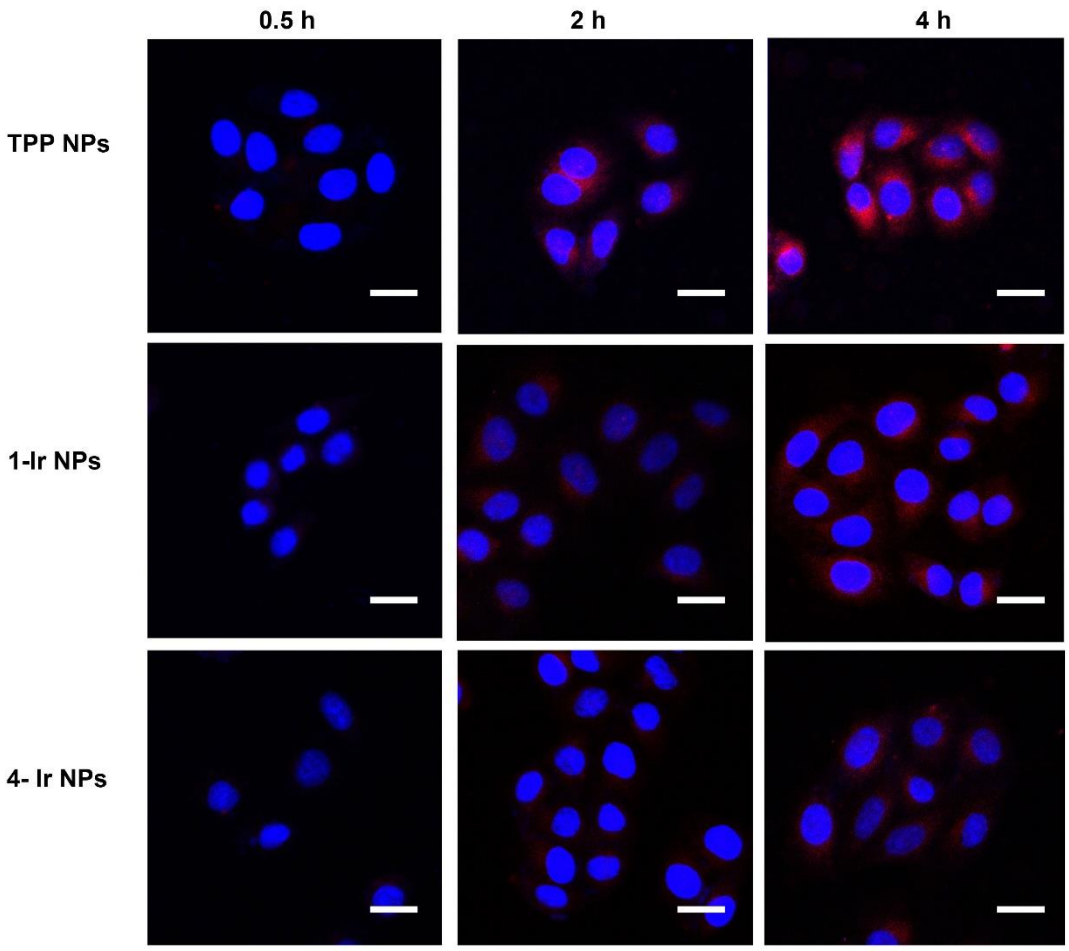

Fig. S33 CLSM images of HeLa cells incubated with **TPP** NPs, **1-Ir** NPs and **4-Ir** NPs (0.5 μM) for 0.5 h, 2 h and 4 h, respectively. Cells are viewed in the blue channel for DAPI, the red channel for NPs. The scale bars are 20 μm.

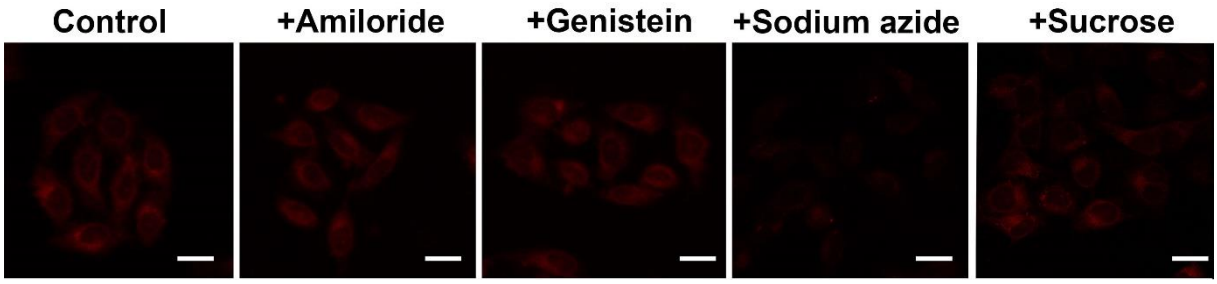

Fig. S34 CLSM images showing HeLa cells incubated with different endocytic inhibitors: none (Control); amiloride (+Amiloride, 13.3 μg m L^{-1}); genistein (+Genistein, 27.024 μg m L^{-1}); sodium azide (+Sodium azide, 1 mg mL^{-1}); and sucrose (+Sucrose, 153.9 mg mL^{-1}). The **4-Ir** NPs was (0.5 μM). The scale bars are 20 μm.

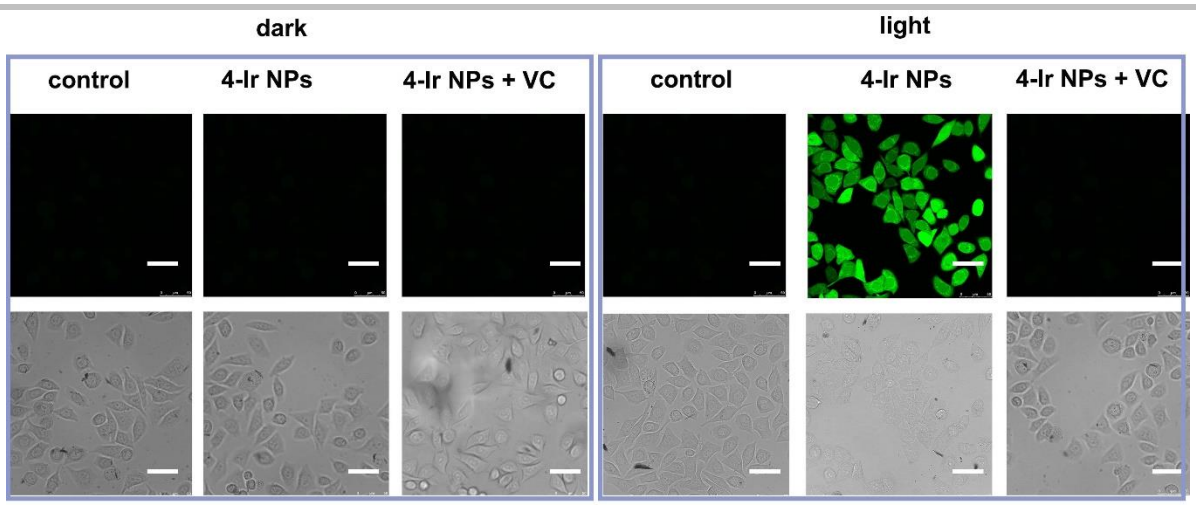

Fig. S35 Generation of intracellular reactive oxygen species (ROS) mediated by **4-Ir** NPs (0.5 μM) upon irradiation (635 nm, 0.6 W cm^{-2}, 3 min) as indicated by the fluorescence of DCFH-DA; the scale bars are 20 μm.

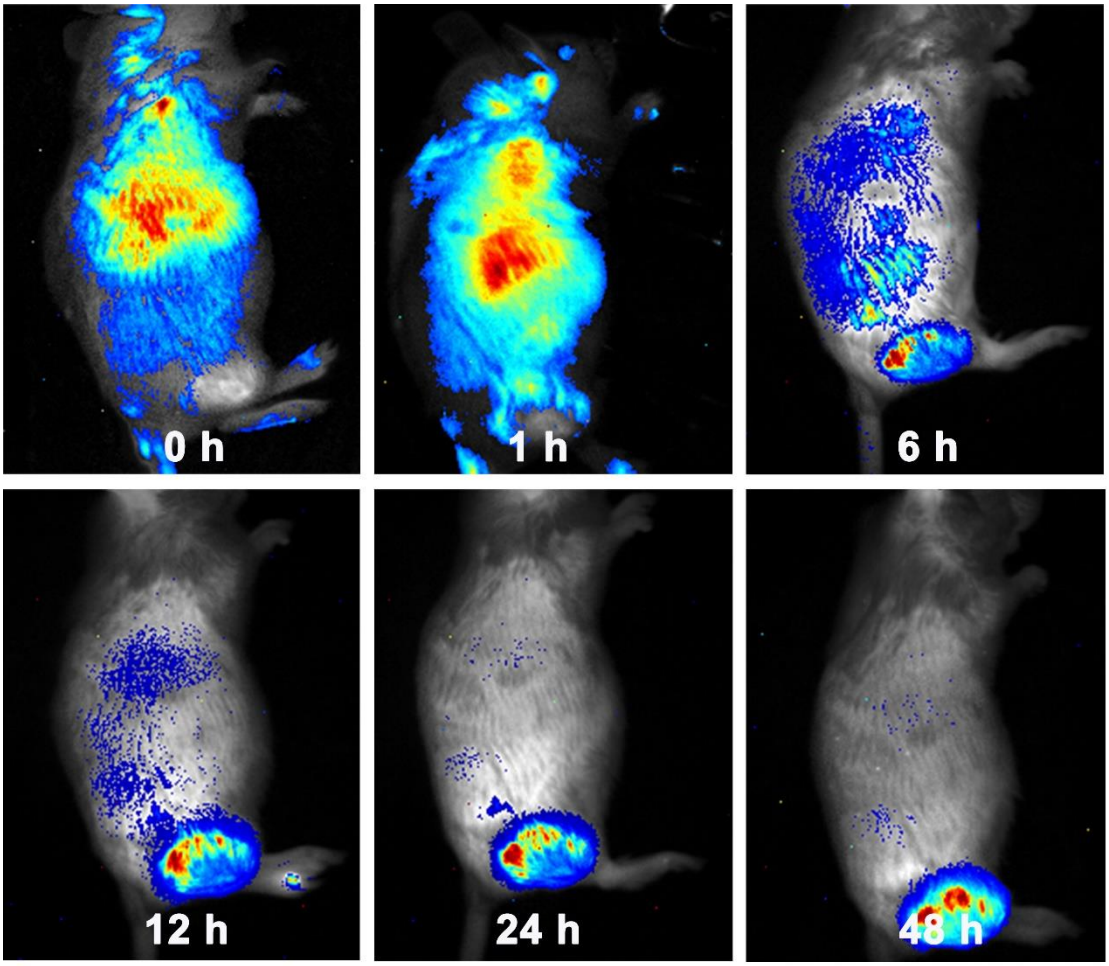

Fig. S36 Time-dependent *in vivo* fluorescence images of U14 tumor-bearing mice after intravenous (IV) injection with IR780-labeled **4-Ir** NPs (100 μg mL^{-1}, 100 μL).

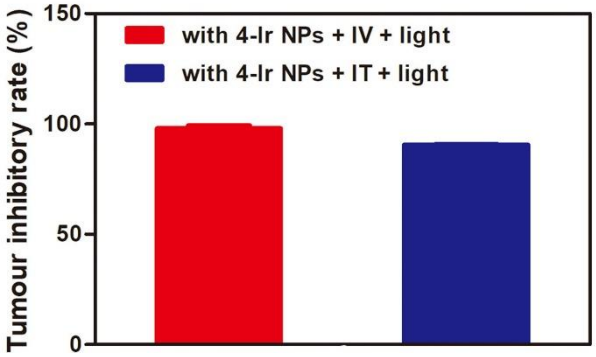

Fig. S37 Tumour-inhibitory rates of mice treated with **4-Ir** NPs + IV (intravenous injection) + Light, and **4-Ir** NPs + IT (intratumoral injection) + Light for 14 days.

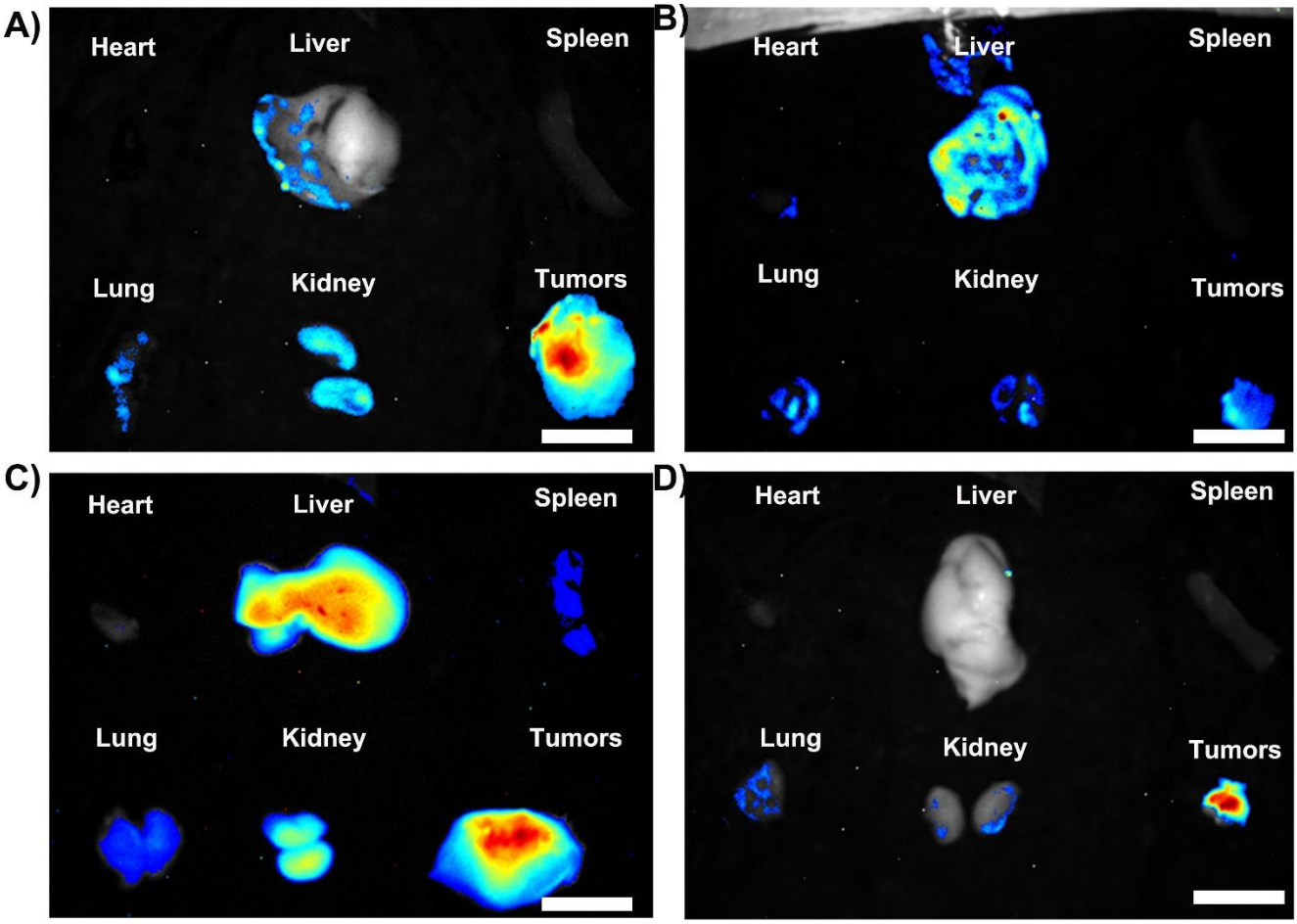

Fig. S38 Fluorescence of major tissues of A) **4-Ir** NPs + IV (intravenous injection), B) **4-Ir** NPs + IV + Light, C) **4-Ir** NPs + IT (intratumoral injection), and D) **4-Ir** NPs + IT + Light for 14 days. The scale bars are 1 cm. The kidneys play a critical role in eliminating reagents out of the body. Therefore, the kidneys have a high accumulation of **4-Ir** NPs after circulation.

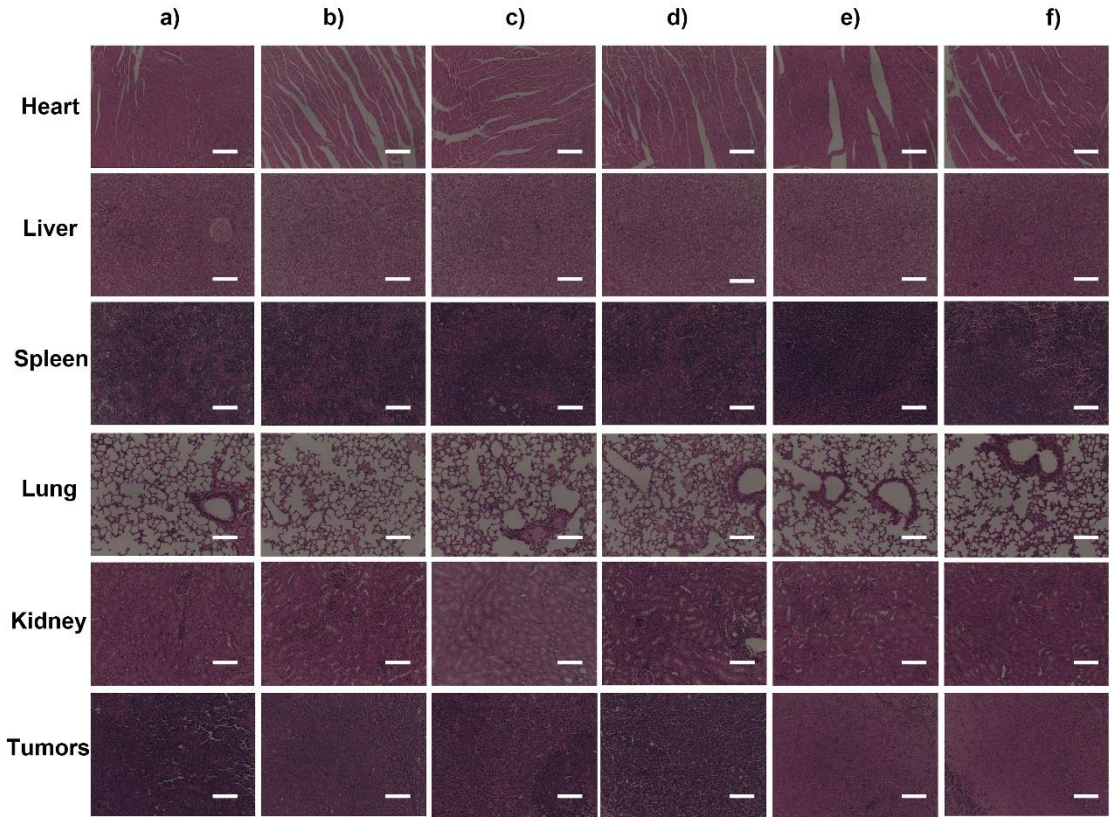

Fig. S39 H&E staining of various organs from mice at the end of experiments after treatment: a) with saline; b) with saline + Light; c) **4-Ir** NPs + IT (intratumoral injection); d) **4-Ir** NPs + IV (intravenous injection); e) **4-Ir** NPs + IT + Light, f) **4-Ir** NPs + IV + Light. The scale bars are 10 μm.

Table S1 The calculated spin-orbital coupling constants (cm^{-1}) between S_n and T_n for **TPP NPs** and **1-Ir NPs** at PBE0/DZP level.

S_n-T_n	**TPP**	**1-Ir**
S_1-T_1	0.2	0.297
S_1-T_2	0.01	0.11
S_1-T_3	0.09	0.15
S_1-T_4	0.003	0.044
S_2-T_1	0.04	0.21
S_2-T_2	0.16	0.21
S_2-T_3	0.006	0.03
S_2-T_4	0.14	0.34
S_2-T_5		4.54
S_3-T_5		12.2
S_3-T_6		7.05
S_4-T_5		9.54
S_4-T_6		4.60
S_5-T_1		5.71
S_5-T_2		10.4
S_5-T_4		5.24
S_5-T_5		106
S_5-T_6		259
S_5-T_7		148

Table S2 Photophysical data of **TPP NPs**, **1-Ir NPs** and **4-Ir NPs**.

	λ_{abs} (nm)	λ_{em} (nm)	Φ_F(%)	T_F (ns)	k_r ($\times 10^7$ s^{-1})	k_{nr} ($\times 10^8$ s^{-1})
TPP NPs	419; 517	655; 719	29	4.32	6.71	1.64
1-Ir NPs	420; 518	657; 720	11	4.67	2.36	1.90
4-Ir NPs	427; 519	660; 724	5	4.82	1.04	1.97

Measured in water at 298 K (1.0×10^{-5} M, λ_{ex} = 527 nm); The radiative k_r and non-radiative k_{nr} values in neat film were calculated according to the equations: $k_r = \Phi/\tau$ and $k_{nr} = (1- \Phi)/\tau$, from the quantum yields Φ and the lifetime τ values.

Table S3 The average diameter and polydispersity index (PDI) results of **TPP NPs**, **1-Ir NPs** and **4-Ir NPs** measured by DLS.

Sample	**TPP** NPs	**1-Ir** NPs	**4-Ir** NPs
Average diameter (nm)	74	79	95
PDI	0.174	0.168	0.170

Table S4 The drug loading content (DLC) and drug loading efficiency (DLE) results of **TPP NPs**, **1-Ir NPs** and **4-Ir NPs**.

Sample	**TPP** NPs	**1-Ir** NPs	**4-Ir** NPs
DLC (mg/mL)	0.146	0.141	0.144
DLE (%)	97.33	94.00	96.02

Author Contributions

L. Z. designed the experiments and the research. Y. G., L. Z., L. L., X. T., S. L. and X. L. performed the experiments. L.Z., Z. S., Z. X. and D. Z. analyzed the data. L.Z., Z. X., D. Z. and M. R. B. wrote the paper. All authors discussed the results and commented on the manuscript.

References

1 Gaussian 16, Revision C.01, M. J. Frisch, G. W. Trucks, H. B. Schlegel, G. E. Scuseria, M. A. Robb, J. R. Cheeseman, G. Scalmani, V. Barone, G. A. Petersson, H. Nakatsuji, X. Li, M. Caricato, A. V. Marenich, J. Bloino, B. G. Janesko, R. Gomperts, B. Mennucci, H. P. Hratchian, J. V. Ortiz, A. F. Izmaylov, J. L. Sonnenberg, D. Williams-Young, F. Ding, F. Lipparini, F. Egidi, J. Goings, B. Peng, A. Petrone, T. Henderson, D. Ranasinghe, V. G. Zakrzewski, J. Gao, N. Rega, G. Zheng, W. Liang, M. Hada, M. Ehara, K. Toyota, R. Fukuda, J. Hasegawa, M. Ishida, T. Nakajima, Y. Honda, O. Kitao, H. Nakai, T. Vreven, K. Throssell, J. A. Montgomery, Jr., J. E. Peralta, F. Ogliaro, M. J. Bearpark, J. J. Heyd, E. N. Brothers, K. N. Kudin, V. N. Staroverov, T. A. Keith, R. Kobayashi, J. Normand, K. Raghavachari, A. P. Rendell, J. C. Burant, S. S. Iyengar, J. Tomasi, M. Cossi, J. M. Millam, M. Klene, C. Adamo, R. Cammi, J. W. Ochterski, R. L. Martin, K. Morokuma, O. Farkas, J. B. Foresman, D. J. Fox, Gaussian, Inc., Wallingford CT, 2016.

2 J. G. Snijders, E. J. Baerends, P. Ros, *Mol. Phys.*, 1979, **38**, 1909-1929.

3 X. Zheng, L. Wang, S. Liu, W. Zhang, F. Liu, Z. Xie, *Adv. Funct. Mater.*, 2018, **28**, 1706507.